| REPORT DOCUMENTATION PAGE | Form Approved OMB No. 0704-0188 |
|---|---|



PLEASE DO NOT RETURN YOUR FORM TO THE ABOVE ADDRESS.

| 1. REPORT DATE *(DD-MM-YYYY)* | 2. REPORT TYPE | 3. DATES COVERED *(From - To)* |
|---|---|---|
| 07-05-2010 | | |

| 4. TITLE AND SUBTITLE | 5a. CONTRACT NUMBER |
|---|---|
| Investigation of Cavity Flow Effects on Store Separation Trajectories | 5b. GRANT NUMBER |
| | 5c. PROGRAM ELEMENT NUMBER |
| 6. AUTHOR(S)<br>Finney, Luke Patrick | 5d. PROJECT NUMBER |
| | 5e. TASK NUMBER |
| | 5f. WORK UNIT NUMBER |

| 7. PERFORMING ORGANIZATION NAME(S) AND ADDRESS(ES) | 8. PERFORMING ORGANIZATION REPORT NUMBER |
|---|---|
| 9. SPONSORING/MONITORING AGENCY NAME(S) AND ADDRESS(ES)<br>U.S. Naval Academy<br>Annapolis, MD 21402 | 10. SPONSOR/MONITOR'S ACRONYM(S) |
| | 11. SPONSOR/MONITOR'S REPORT NUMBER(S)<br>Trident Scholar Report no. 388 (2010) |

12. DISTRIBUTION/AVAILABILITY STATEMENT

This document has been approved for public release; its distribution is UNLIMITED

13. SUPPLEMENTARY NOTES

14. ABSTRACT

In this study, a cavity previously used as part of the Navy Internal Carriage and Separation (NICS) experiments will be used in conjunction with the Mark 82 (500 lb class) store to compare previously obtained wind tunnel data to CFD results for an internal bay/store configuration. Forces and moments for the store along the horizontal traverse will be found using a specific single equation turbulence model (Spalart-Allmaras) in order to better understand the nature of the flow and its affect on the store with an emphasis on the region in the vicinity of the shear layer. The CFD results will be compared with existing wind tunnel data on the same configurations in order to judge the efficacy of using Euler, Navier-Stokes, and time-accurate Navier-Stokes flow solvers to provide mean force data for the store.

15. SUBJECT TERMS

Navy Internal Carriage and Separation Experiment, Store Separation, Computational Fluid Dynamics, Spalart-Allmaras turbulence model

| 16. SECURITY CLASSIFICATION OF: | | | 17. LIMITATION OF ABSTRACT | 18. NUMBER OF PAGES | 19a. NAME OF RESPONSIBLE PERSON |
|---|---|---|---|---|---|
| a. REPORT | b. ABSTRACT | c. THIS PAGE | | 78 | 19b. TELEPHONE NUMBER *(Include area code)* |

U.S.N.A. --- Trident Scholar project report; no 388.

**Investigation of Cavity Flow Effects on Store Separation Trajectories**

by

Midshipman 1/C Luke P. Finney, USN
United States Naval Academy
Annapolis, Maryland

_____
(signature)

Certification of Adviser Approval

Assistant Professor Eric N. Hallberg
Aerospace Engineering Department

_____
(signature)

_____
(date)

Acceptance for the Trident Scholar Committee

Professor Carl Wick
Deputy Director of Research & Scholarship

_____
(signature)

_____
(date)

USNA-1531-2

# ABSTRACT

Summary Statement

**Summary**

In order to establish safe flight conditions for the release of bombs or other stores from attack aircraft, the Navy conducts flight tests at various aircraft attitudes, Mach numbers, and store configurations and determines the initial path taken by the falling store. This determination of path is generally made using a series of high speed photographs, known as photogrammetrics, or the analysis of data taken from an accelerometer located on the store itself, known as telemetry. Though very accurate, many such flight tests are necessary in order to approve a range of acceptable flight conditions, and these are costly in both time and money.

The number and duration of flights required can be significantly reduced by predicting trajectories before flights are begun. These predictions are made using store separation analysis, which is a branch of aerodynamics concerned with the trajectories of bombs, missiles and fuel tanks immediately after they are detached from the host aircraft. This field is very important as these stores do not necessarily move downward. There have been cases where the store actually moved up or sideways and impacted the releasing aircraft, occasionally causing extensive damage. Store separation analysis can be used to identify these high-risk release conditions prior to encountering them during flight tests.

Prevention of this problem lies with extensive pre-flight flow analysis, accomplished both in the wind tunnel and through computational fluid dynamics (CFD). Prior to any flight testing, predicted trajectories are obtained using one or both of these methods, and these results are used to determine which configurations require flight tests and to what extent. For instance, a clearance to Mach 1 may require a build-up approach beginning at a benign flight condition such as Mach 0.8 and progressing up to Mach 1 at steps of 0.02 Mach. Extensive wind tunnel and CFD analysis could permit fewer steps in the build-up to the end point if CFD and wind tunnel

analysis shows the endpoint to be safe, and interim flight test steps match predictions.

The application of CFD to store separation is not a new concept. Research in this area began in the late 1970s, and with ever increasing computational power the use of CFD to reduce the total number of flight and wind tunnel tests has become more and more feasible. A series of successful CFD challenges in the 1990's focused on predicting the trajectory of stores released on external pylon stations. Recently, store separation engineers have begun to apply CFD techniques to store separations from bomb bays. The Unmanned Combat Air System (N-UCAS) and F-35 Joint Strike Fighter are two aircraft programs with weapons bays that come to mind. As a result of these and earlier programs, such as the B-1B Lancer and B-2 Spirit Air Force aircraft program, stores released from internal bays have become an important focus of research in the store separation community.

Cavity flow is fundamentally unsteady, but stores must be released and separated in a predictable manner. Previous research has looked extensively at the acoustics of the cavity as a measure of the unsteady flow. Other research has looked at the vertical position of the store within the cavity and the effect of this depth on the aerodynamic forces on the store. Not surprisingly, the aerodynamic forces often go to near zero as the store is raised higher in the bay away from the cavity opening, especially for deep bays. When the flow velocities are small, the trajectory of the bomb is solely influenced by the ejector force and gravity. However, in the regions of the flow where velocities are high, the trajectory of the store will be influenced and changed to varying degrees. One of these high-speed regions is the boundary between the cavity and the external free-stream. This high-speed region, termed the shear layer, is not well understood since unsteady pressure measurements, usually captured by acoustic data, are always taken at the surface of the cavity. Furthermore, it is known that the shear layer is not two-dimensional, i.e. flat and parallel to the cavity opening. Various other studies have pointed to the shear layer at the boundary of the cavity as the major contributor to adverse separation influences. Passive control of the cavity flow is typically accomplished through devices such as spoilers and ejector mechanisms to alleviate unsteady and highly three-dimensional aspects of the shear layer. New aircraft programs, however, are proposing cavities without these flow

control devices for operational reasons.

Wind tunnel data exists from a previous study which measured the forces on the store along a horizontal traverse in and out of the bay at a number of depths. No other data of this type is available for similar transonic flight conditions and it is felt that this information can be used to assess the ability of CFD to capture the effects of the shear layer on the store.

Abstract

Computational Fluid Dynamics is an integral part of flight testing and clearances for store separation problems. Trajectories of stores released from internal weapons bays have been shown in recent tests to diverge from predicted paths. It is critical to develop an accurate method of predicting the trajectory for a range of store configurations. The use of CFD to model the unsteady flow that is present inside and immediately around the weapons bay is both time consuming and problematic. The effect of this flow has the potential to make the store trajectories unrepeatable; an unacceptable condition for the purposes of providing a flight clearance for a particular configuration. Store separation analysis based on CFD has the potential to show significant savings in terms of cost and schedule for future weapons programs especially for complex store releases such as those released from a weapons bay. However, it is not feasible to computationally assess every release condition. This work will help provide guidance as to where computationally expensive CFD calculations need to be performed and where they do not for stores released from similar cavities.

In this study, a cavity previously used as part of the Navy Internal Carriage and Separation (NICS) experiments will be used in conjunction with the Mark 82 (500 lb class) store to compare previously obtained wind tunnel data to CFD results for an internal bay/store configuration. Forces and moments for the store along the horizontal traverse will be found using a specific single equation turbulence model (Spalart-Allmaras) in order to better understand the nature of the flow and its affect on the store with an emphasis on the region in the vicinity of the shear layer. The CFD results will be compared with existing wind tunnel data on the same configurations in order to judge the efficacy of using Euler, Navier-Stokes, and time-accurate

Navier-Stokes flow solvers to provide mean force data for the store.

The results of the CFD solutions will serve as input to the Navy Generalized Separation Package (NAVSEP), which combines the aerodynamic forces and moments, ejector and gravitational forces and the restricted motion properties of the store in order to predict the trajectory of the store after release. The store mass properties and ejector force profiles will be varied for the range of aerodynamic forces predicted by CFD. The family of resulting trajectories will be used to draw conclusions as to the extent to which the unsteady nature of the cavity flow can be expected to adversely affect the trajectory of the store.

Keywords: store separation, computational fluid dynamics, Navy Internal Carriage and Separation, unsteady cavity flow, trajectory modeling

# ACKNOWLEDGEMENTS

First, I would like to thank my advisor, Assistant Professor Eric Hallberg, whose drive, dedication, guidance, enthusiasm, professionalism, sarcasm, humor, and refreshing bluntness were essential to the execution of this project. I would also like to thank Dr. Alex Cenko of Naval Air Systems Command for his guidance and expert knowledge in the area of research.

Next, I would like to thank Ms. Linda Adlum for her un-measurable help with the technical expertise, her candid advice and overall understanding of the intricacies of the Linux cluster at the Naval Academy.

Finally, I would like to thank Professor Carl Wick and the Trident Scholar Committee for their constructive input and the opportunity to conduct this research while allowing me to have the space to determine my own work schedule.

# TABLE OF CONTENTS

# LIST OF FIGURES

## LIST OF TABLES



## LIST OF SYMBOLS

6DOF ..... six degrees of freedom
ATFLIR ..... Advanced Targeting Forward Looking Infrared Pod
CFD ..... Computational Fluid Dynamics
JDAM ..... Joint Direct Attack Munition
NAVAIR ..... Naval Air Systems Command
NAVSEP ..... Navy Generalized Separation Package
TFLIR ..... Targeting Forward Looking Infrared Pod
$C_x$ ..... axial force coefficient
$C_y$ ..... sideforce coefficient
$C_z$ ..... normal force coefficient
$C_l$ ..... rolling moment coefficient
$C_m$ ..... pitching moment coefficient
$C_n$ ..... yawing moment coefficient
$C_p$ ..... pressure coefficient

# INTRODUCTION

## Nomenclature

| | |
|---|---|
| 6DOF | 6 Degree of Freedom |
| ADEC | Arnold Engineering Development Center |
| ACFD | Applied Computational Fluid Dynamics |
| CFD | Computational Fluid Dynamics |
| GRIDTOOL | TetrUSS Geometry Creation Application |
| JDAM | Joint Direct Attack Munitions |
| NAVSEP | Navy Generalized Separation Package |
| NICS | Navy Internal Carriage and Separation |
| TetrUSS | Tetrahedral Unstructured Software System |
| USM3D | Unstructured Viscous Tetrahedral Flow Solver |
| VGRID | TetrUSS Volume Grid Creation Application |
| WICS | Weapons Internal Carriage and Separation |

## Background

In order to establish safe flight conditions for the release of ordnance or other stores from attack aircraft, the Navy conducts flight tests at various aircraft attitudes, Mach numbers, and store configurations and determines the initial path taken once the store is released. The determination of the initial trajectory is generally made using a series of high speed photographs, known as photogrammetrics, or through the processing of data taken from an inertial measurement unit located on the store itself, known as telemetry. Though very accurate, many such costly flight tests are necessary in order to approve a range of acceptable flight conditions.

The number and duration of flights required can be significantly reduced by predicting trajectories using engineering methods outside of flight test. These predictions are made using store separation analysis, which is a branch of aerodynamics concerned with the trajectories of

bombs, missiles and fuel tanks immediately after they are detached from the carriage aircraft. Due to the large loads imparted on the store from the air, these stores do not necessarily move downward. In extreme cases, the store may move up or sideways and impacted the releasing aircraft, potentially causing extensive damage. Store separation analysis can be used to identify these adverse release conditions prior to encountering them during flight tests.

Prevention of this problem lies with extensive pre-flight flow analysis, accomplished both in the wind tunnel and through computational fluid dynamics (CFD). Prior to any flight testing, predicted trajectories are obtained using one or both of these methods, and these results are used to determine which configurations require flight tests and to what extent. For instance, a clearance to Mach 1 may require a build-up approach beginning at a benign flight condition such as Mach 0.8 and progressing up to Mach 1 at steps of 0.02 Mach. Extensive wind tunnel and CFD analysis could permit fewer steps in the build-up to the end point if CFD and wind tunnel analysis shows the endpoint to be safe, and interim flight test steps match predictions.

A number of modern combat aircraft release stores from internal weapons bays. The Unmanned Combat Air System (UCAS), F-35 Joint Strike Fighter, P-8A and the F-22 aircraft programs rely upon weapons bays to complete their mission. As a result of these and earlier programs, such as the B-1B Lancer and B-2 Spirit Air Force aircraft programs, stores released from internal bays have become an important focus of research in the store separation community.

The fluid dynamic nature of a weapons bay is complex and fundamentally unsteady. A store will experience different forces depending upon the time of release. The trajectory of a store seems to be most heavily influenced by its interaction with the boundary between the cavity and the external freestream. This region, termed the shear layer, is not as well understood since unsteady pressure measurements (acoustics) are always taken at the surface of the cavity. Furthermore, it is known that the shear layer is not two-dimensional, i.e. flat and parallel to the cavity opening. The studies have pointed to the shear layer at the boundary of the cavity as the major contributor to adverse separation influences. Passive control of the cavity flow has typically been accomplished through the use of devices such as spoilers and ramps.

Additionally, ejector mechanisms are used to alleviate the influence of the unsteady and highly three-dimensional aspects of the shear layer. The vorticity of the shear layer and the effects of a passive control can be seen in Figure 1. New aircraft programs, however, are proposing cavities without spoilers or ramps for operational reasons. Store releases must still be predictable and repeatable in order to issue a flight clearance. Therefore, further analysis is required to understand the implications of removing these devices.

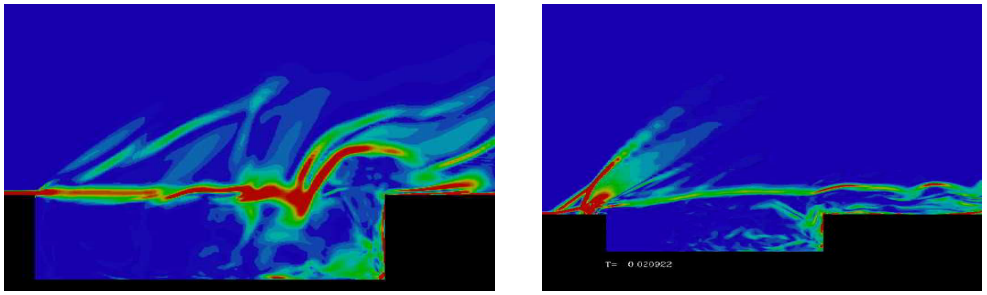

**Figure 1. Shear layer and shear layer with passive control**

The influence of the unsteady flow upon the store and its trajectory has been looked at through many different methods. Previous research using wind tunnels has looked extensively at the acoustics of the cavity as a measure of the unsteady flow. The limitation and disadvantage of this research is that the measurements are taken only on the cavity surfaces. The degree of correlation between these measurements with aerodynamic forces on the store at specific locations within the bay is not necessarily good. Extensive wind tunnel research has been accomplished for different trajectories from weapons bays, most notably the Weapons Internal Carriage and Separation (WICS) tests, conducted by the Air Force during the 1990's. The Arnold Engineering Development Center (AEDC) established a database for internal carriage and release of stores. Three tests were conducted at transonic and supersonic conditions, cataloguing aerodynamic loads on store models at a grid of locations within the cavity, surface pressure distributions on the cavity walls and on the store, and separation trajectories for stores. The generic cavity and stores used were specific to the Air Force with the focus on shallow bays and slender (air-to-air ordinance) weapons. But, some tests were done at a bay length to height (L/H) ratio of 4.5 which was the same as the Navy Internal Carriage and Separation (NICS) test program, shown in Figure 2. Unique to the Navy effort, tests were run on a model Mark 82 (air-to-ground ordnance) at various positions within the cavity. These tests are distinctive because the

data is taken along a horizontal traverse of the cavity at different depths. Of note, the data from the NICS testing has never been compared to results from CFD.

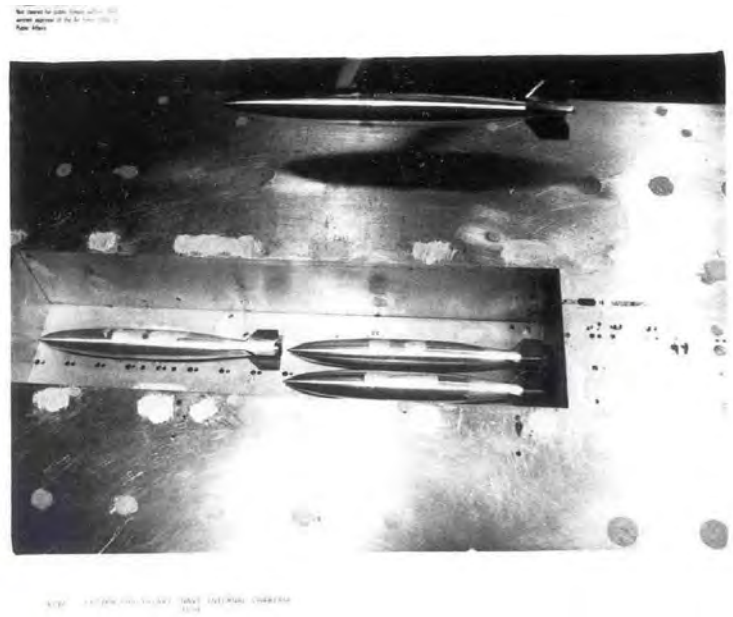

**Figure 2. NICS Cavity Configuration**

CFD research has looked at the store separation problem from various different aspects as well. Results from acoustic data have been compared with wind tunnel and flight test. Flow fields around different size cavities and using different CFD method have been developed and analyzed. Methods such as the Detached Eddy Simulation (DES) and Large Eddy Simulation (LES) have been advanced, as well as turbulence modeling in the boundary layer, approximated through the Spalart-Allmaras (S-A) model. However, the opportunity to validate these computational simulations has not always been available by equivalent wind tunnel or flight test data. Nor have different common computational methods been compared for relative accuracy in predicting store loads for configurations representative of strike aircraft (air-to-ground ordnance). In addition, most research has looked at the vertical position of the store within the cavity and the effect of this depth on the aerodynamic forces on the store. Not surprisingly, the aerodynamic forces often go to near zero as the store is raised higher in the bay away from the cavity opening, especially for deep bays. The change in forces upon the store as it is moved forward and aft within the bay has not been studied using computational methods, and it is believed that an analysis along a horizontal traverse will help to characterize the shear layer.

Realistically, the effect of flow unsteadiness upon the store's trajectory is case dependent. The magnitude of the aerodynamic forces must be significant relative to the inertial and ejector loads in order to affect the motion of the store. Cenko, Deslandes, Killenius and Stanek also discussed the fact that computational techniques are inadequate for producing realistic loads given that the unsteadiness is difficult to analyze.

Furthermore, it is not known whether steady flow solutions can capture the average effect of the unsteady flow. An important element of this research would be to determine how well a steady flow solution of a cavity flow configuration predicts the store loads. The metric for comparison will be the wind tunnel test data from the NICS tests.

Wind tunnel data exist from the previous NICS study which measured the forces on the store along a horizontal traverse in and out of the bay at a number of depths. No other data of this type are available for similar transonic flight conditions and it is felt that it can be used to assess the ability of different CFD methods to capture the effects of the shear layer on the store. While the flow deep in the bay is unsteady, it is also lower in velocity and its affect on the store is much less than that of the flow in the shear layer. The shear layer may be an essentially steady phenomenon with its effect able to be predicted using computational steady flow methods. This is essentially what is done in wind tunnel testing when store loads are determined from time averaged readings. It is felt that a comparison of steady and unsteady flow solutions to the store loads measured in the NICS wind tunnel test will help to characterize the efficacy and applicability of these methods for similar configurations in the future.

## Method of Investigation

This project will investigate the use of CFD techniques to accurately predict trajectories of a store. These predictions will be validated through comparison with previously obtained wind tunnel tests. The relative influence of the effects of the shear layer on a store compared to the inertial and ejector forces will be evaluated. This will show the point at which unsteady aerodynamic flow makes significant changes to the store trajectory. The shape of the shear layer

will also be characterized by the effects on the store seen along the longitudinal axis of the cavity. CFD techniques using steady flow solutions will be compared to CFD techniques using unsteady (time-accurate) flow solutions in order to determine if the former accurately capture the behavior of the shear layer when it is essentially steady. The forces and moments calculated by the CFD will be used to compute trajectories based upon external variables.

## Experimental Process

The CFD predictions will be compared with the NICS data through an analysis of the forces and moments imparted on the store at each configuration. In order to obtain this data with CFD, the models must be created computationally using geometric grids. Once built, they will be tested in free-stream conditions to ensure the aerodynamic behavior is the same as the physical model tested. Once it is verified that the stores have been adequately modeled, the various bay configurations will be constructed. Flow solutions will be obtained using commonly used computational methods in order to obtain pressure distributions on the model. Pressure distributions are integrated in order to obtain the forces and moments on the store and these numbers are then compared with those from the previous wind tunnel testing. These numbers will also be used to characterize the shear layer strength at various points along the longitudinal axis. The forces and moments on the store are then put into Navy Generalized Separation Package (NAVSEP) along with ejector and inertial forces. The force and moment data on the store serve as input to a trajectory generation program termed NAVSEP. This program is used to calculate a trajectory of the store after release based, in part, on this data. The ejector and inertial forces will be varied in a parametric fashion in order to determine when variations in the aerodynamic forces significantly affect the trajectory. Figure 3 is a diagram of the process described above.

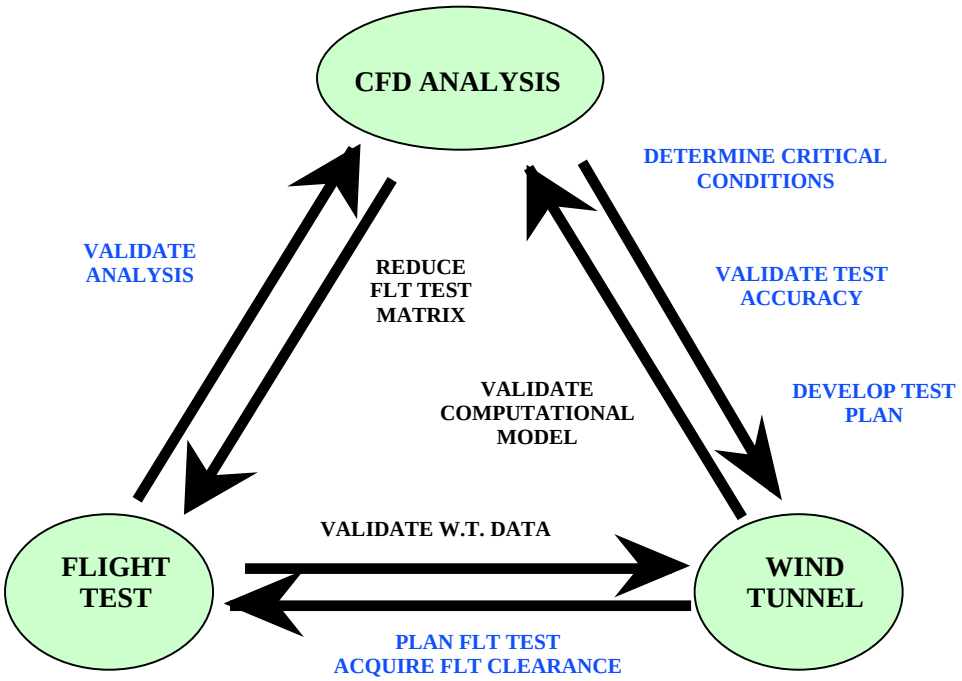


**Figure 3. Diagram of CFD Process**

## Comparison Data

Wind tunnel tests have been conducted using the Navy Internal Carriage and Separation (NICS) cavity seen in Figure 2.The forces and moments on the Mark 82 were measured using the captive trajectory system as it traversed the longitudinal axis of the cavity at several different bay depths. The data from these tests have never been previously analyzed and provide an invaluable source of information. This geometry of this configuration will be computationally reproduced and used to generate unstructured grids for the purposes of computing flow solutions using CFD. The CFD solutions will be found at the same grid locations evaluated in the wind tunnel tests as shown below in Figure 4. It is felt that a comparison of increasing computationally intensive CFD flow solutions to the existing wind tunnel data will yield insight as to the ability of each method to capture the effects of the flow on the store.

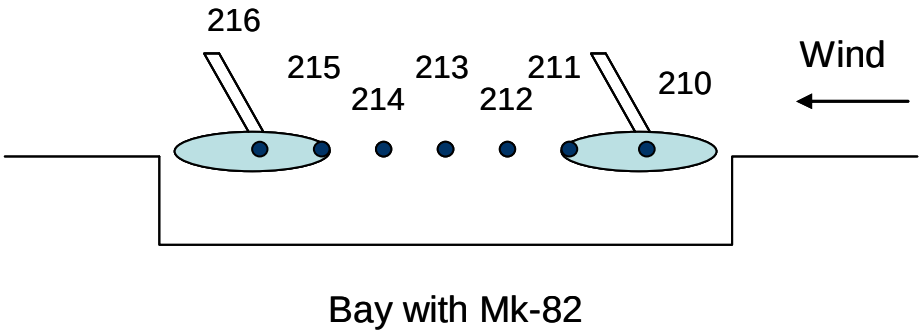


**Figure 4. Configurations Tested for the CFD Comparison to NICS**

# COMPUTATIONAL METHODS

## CFD Development

Computational fluid dynamics is based on three fundamental physical principles given in equation form below. These principles are conservation of mass, conservation of momentum, and conservation of energy.[1] There are multiple forms of each equation, each used for different problems. Shown below in Equation 1 through Equation 3 are the governing equations for an unsteady, compressible, viscous flow.

Conservation of mass:

$$\frac{\partial \rho}{\partial t} + \nabla \cdot (\rho V) = 0$$

Equation 1

Conservation of momentum:

$$\frac{\partial (\rho u)}{\partial t} + \nabla \cdot (\rho u V) = -\frac{\partial p}{\partial x} + \frac{\partial \tau_{xx}}{\partial x} + \frac{\partial \tau_{yx}}{\partial y} + \frac{\partial \tau_{zx}}{\partial z} + \rho f_x$$

$$\frac{\partial (\rho v)}{\partial t} + \nabla \cdot (\rho v V) = -\frac{\partial p}{\partial y} + \frac{\partial \tau_{xy}}{\partial x} + \frac{\partial \tau_{yy}}{\partial y} + \frac{\partial \tau_{zy}}{\partial z} + \rho f_y$$

$$\frac{\partial (\rho w)}{\partial t} + \nabla \cdot (\rho w V) = -\frac{\partial p}{\partial z} + \frac{\partial \tau_{xz}}{\partial x} + \frac{\partial \tau_{yz}}{\partial y} + \frac{\partial \tau_{zz}}{\partial z} + \rho f_z$$

Equation 2

[1] Anderson, John D., Computational Fluid Dynamics: The Basics with Applications. New York: McGraw-Hill, Inc., 1995, p 38.

Conservation of energy:

$$\frac{\partial}{\partial t}\left[\rho\left(e+\frac{V^2}{2}\right)\right]+\nabla\cdot\left[\rho\left(e+\frac{V^2}{2}\right)V\right]=\rho\dot{q}+\frac{\partial}{\partial x}\left(k\frac{\partial T}{\partial x}\right)+\frac{\partial}{\partial y}\left(k\frac{\partial T}{\partial y}\right)+\frac{\partial}{\partial z}\left(k\frac{\partial T}{\partial z}\right)$$
$$-\frac{\partial(up)}{\partial x}-\frac{\partial(vp)}{\partial y}-\frac{\partial(wp)}{\partial z}+\frac{\partial(u\tau_{xx})}{\partial x}+\frac{\partial(u\tau_{yx})}{\partial y}+\frac{\partial(u\tau_{zx})}{\partial z}+\frac{\partial(v\tau_{xy})}{\partial x}+\frac{\partial(v\tau_{yy})}{\partial y}+\frac{\partial(v\tau_{zy})}{\partial z}$$
$$+\frac{\partial(w\tau_{xz})}{\partial x}+\frac{\partial(w\tau_{yz})}{\partial y}+\frac{\partial(w\tau_{zz})}{\partial z}+\rho f\cdot V$$

Equation 3

This set of equations was first compiled independently by M. Navier and G. Stokes at the beginning of the 19th century, and are thus known as the Navier-Stokes equations.[2] A simpler version of these equations that does not include viscous forces was formulated by Euler and is also frequently used in CFD applications.

$$\frac{\partial\rho}{\partial t}+\nabla\cdot(\rho V)=0 \text{ (Mass)}$$

$$\frac{\partial\rho}{\partial t}+\frac{\partial(\rho V)}{\partial x}=-\frac{\partial p}{\partial x} \text{ (Momentum)}$$

$$\frac{\partial\rho h}{\partial t}+\frac{\partial(\rho hV)\tau_{xy}}{\partial x}=\frac{\partial p}{\partial t}+V\frac{\partial p}{\partial x} \text{ (Energy)}$$

Equations 4, 5 and 6

There is no known analytical solution to these equations, and as such all solutions to the equations are numerical approximations.

The method used to find numerical solutions to these equations is called discretization, a term that means the properties of the airflow are calculated at a finite number of points in a given volume. The large volumes must be broken into many different smaller pieces, or cells in order for the equations to be accurately solved for the volume. The method by which the cells are made is an important process known as grid generation.

---

[2] Anderson, John D., Computational Fluid Dynamics: The Basics with Applications. New York: McGraw-Hill, Inc., 1995, p 64.

## TetrUSS

This research project has employed the NASA-developed Tetrahedral Unstructured Software System (TetrUSS) for CFD analysis. This software package is a suite of three different programs, each of which is used in a different step of the process. TetrUSS is a tetrahedral-based, unstructured flow solver which uses USM3D 6.0 CFD code. It constitutes four software tools which will be used sequentially to generate necessary aerodynamic data. It is advertised as a "loosely integrated, flexible aero analysis and design system."[3] It is a tetrahedral cell-centered, finite volume CFD program that uses the perfect gas model. Some of its more distinguished attributes are a parallel execution capability, a variable time step and integration capacity, and support of numerous different turbulence models, including the Spalart Allmaras as well as the Algebraic Reynolds Stress Model. The Spalart Allmaras turbulence model was conceived in the early 1990's and uses a single equation approximation for the viscosity of the fluid at the boundary layer. The velocity gradient at the surface of an object is difficult to accurately resolve, especially in cavity flow problems. As the air detaches from the surface at the leading edge of the cavity, the surface viscosity effects become very complex. A significant portion of the results of this project depend upon the ability of this approximation to solve the complex cavity flow. It solves a transport equation for a viscosity-like variable.[4] There are multiple utilities available in order to transfer and manipulate the large data files that are formed from the solutions. It was developed at NASA's Langley Research Center and won software of the year awards in 1996 and 2004.

[3] What is TetrUSS Powepoint, www.tretruss.com Accessed 20 November 2009.
[4] CFD Online. www.cfd-online.com. Accessed 12 April 2010.

### *Geometry Generation and Manipulation (GridTool)*

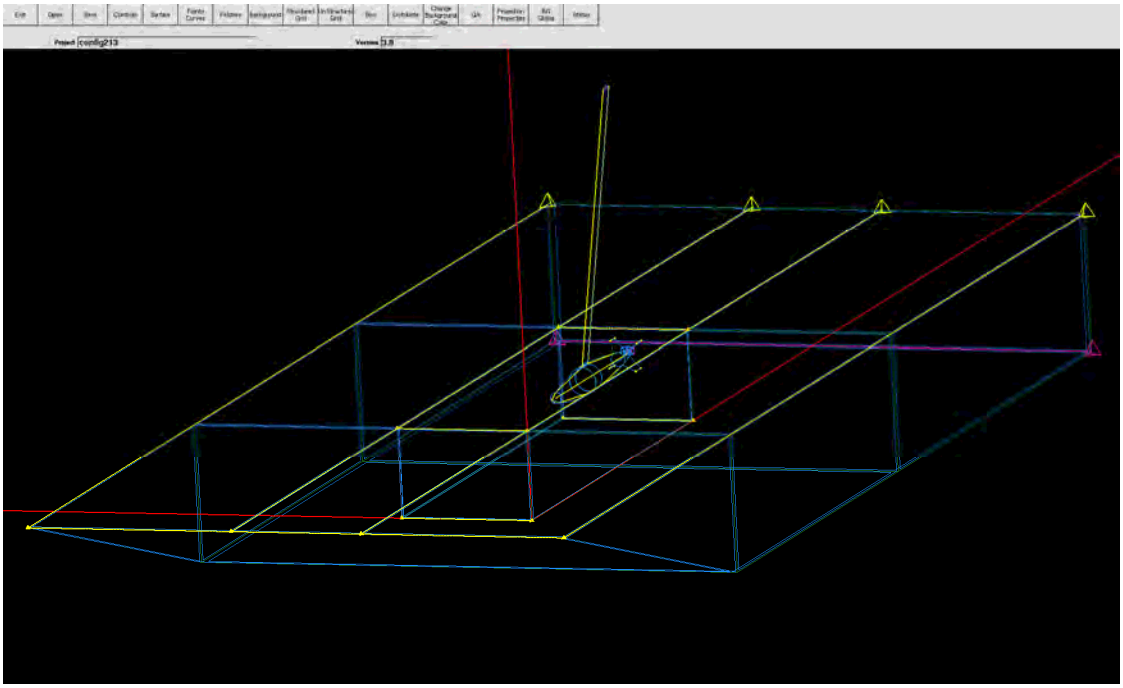

**Figure 5. GridTool Wireframe Cavity and Store**

The first step in the process of store trajectory computation is concerned with generating the appropriate geometry models for the configuration of interest. Rough geometry files exist for both stores, but these are not suitable for use in CFD applications. The NICS cavity has the engineering drawings available used to build the wind tunnel test article but does not have geometry available in electronic form. TetrUSS contains a geometry application called GridTool, which was used to take the rough store geometries and produce watertight geometries suitable for gridding. Other CAD and solid modeling software tools such as Solidworks and Rhino were used as needed to produce IGS files that can be imported into GridTool. GridTool was used to 'patch' the surface of the geometric model such that further programs are able to be used for unstructured grid generation. It is critical that all surfaces are watertight, or the flow solver will allow airflow into the interior of the body, creating a mathematical inconsistency and rendering the flow solver useless. Figure 6 below shows best the different patches that were placed on surfaces, indicated by the different colors. Turning the geometric models into the appropriate patches and surfaces consumed the majority of the time in this step.

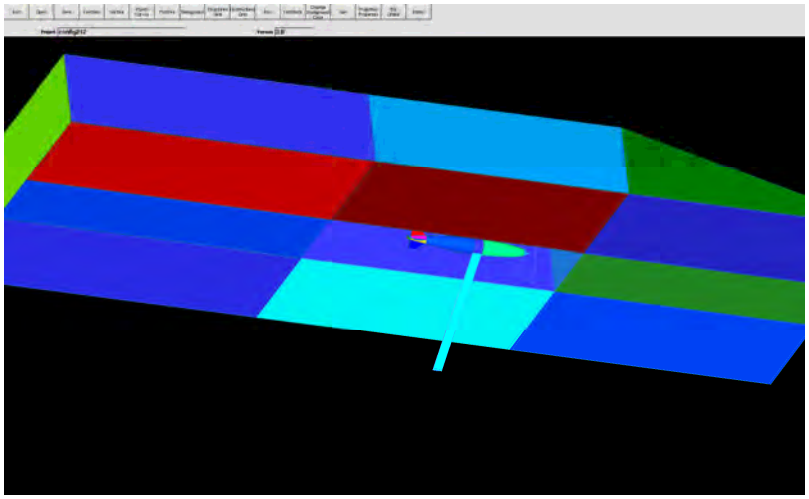

**Figure 6. GridTool Shaded Cavity and Store**

The model was broken into different pieces, defined by a number of lines and points, then a surface was created from that section. From the surface, the patch was made to cover the same area. A patch is a bounded surface used to define the outer boundary of the geometry which transfers direction and coordinates to the grid generation program, VGrid. The patch outlines can also be seen in Figure 5 as evidenced by the blue lines. Additionally, GridTool provides the methodology to determine the grid sizing and various required boundary conditions as dictated by the problem at hand. This is accomplished by defined directions on the surface patches. The arrow in Figure 7 shows the direction in which to grow the grid.

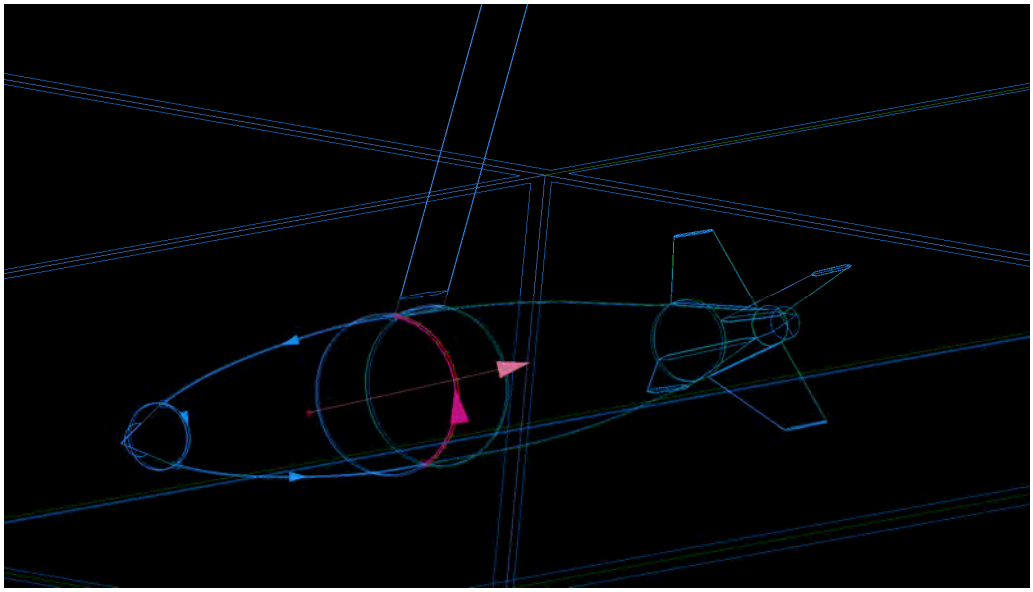

**Figure 7. GridTool Mk-82 Patches**

Another necessary parameter specified by GridTool is the creation of the background source grid. This source grid determines the size of the cells created to partition the larger patches into flat tetrahedral cells to model the actual geometry. These sources are specified by either line or point sources, seen in Figure 5 as the yellow lines and triangles. They have both different sizes and magnitudes of influence, specified through GridTool. The placement of the sources is critical, as they determine the level of resolution in the volume grid and ultimately the final solution. In areas of complex flow, where the properties of the air change quickly, it is necessary to have small cells to capture those changes accurately. The cavity has a number of these high complexity areas because of the right angles present, and the cavity itself. However, in areas of stable, less complex flow such as the flat surface on the bottom of the model, it is advisable to create large cells for faster computation. Once complete, the data files with the positions of points and patches are transferred to the VGrid program for grid creation.

**Table 1. Grid Geometry Properties**

| Model | # of Curves | # of Sources | Surfaces | Patches |
|---|---|---|---|---|
| Mk-82 | 114 | 27 | 36 | 53 |
| Mk-82 with strut | 122 | 29 | 37 | 57 |
| Cavity | 59 | 18 | 24 | 29 |
| Cavity with Mk-82 | 158 | 53 | 61 | 80 |

### *Surface and Volume Grid Generation (VGRID)*

The next program used to prepare the model for the flow solution is called VGRID. This utilizes the files created by GridTool to break the model surface up into small tetrahedral cells then expands that surface grid to fill the specified volume.

There are two categories of grid generation, structured and unstructured. As can be seen in Figure 8, the sizes of the tetrahedrons in the grid vary depending on location. This is because TetrUSS software is based on unstructured grid development, meaning that the size and shape of individual elements can be changed by the user in order to create a complete grid. When developing surface grids, the engineer specifies very small elements for areas of fine detail and sharp curves, and larger grids for areas with little change in geometry or airflow. This method maintains high form integrity while requiring much less computing time than equivalent structured grids would. For this project the grid geometry surrounding the NICS cavity and the Mk-82 was constructed using the Linux servers here at the Naval Academy.

The other category of grid, structured, has a particular set of different advantages and disadvantages. The cells have an order; they must be rectangular and equally spaced in a grid. While different areas of the grid can be made of smaller cells, the grid is inherently inflexible. The order of the grid simplifies calculations and computing, but is labor intensive when used to model complex shapes. The grid creator has excellent control of the grid and can designate areas of smaller cells, but creating such a grid is very time consuming. Because of the speed and ease in creating unstructured grids as compared to a structured grid, the unstructured grids were used in this experiment. In addition, unstructured grids offer unintended breakthroughs in understanding the nature of computation in the areas of complex aerodynamic flow.

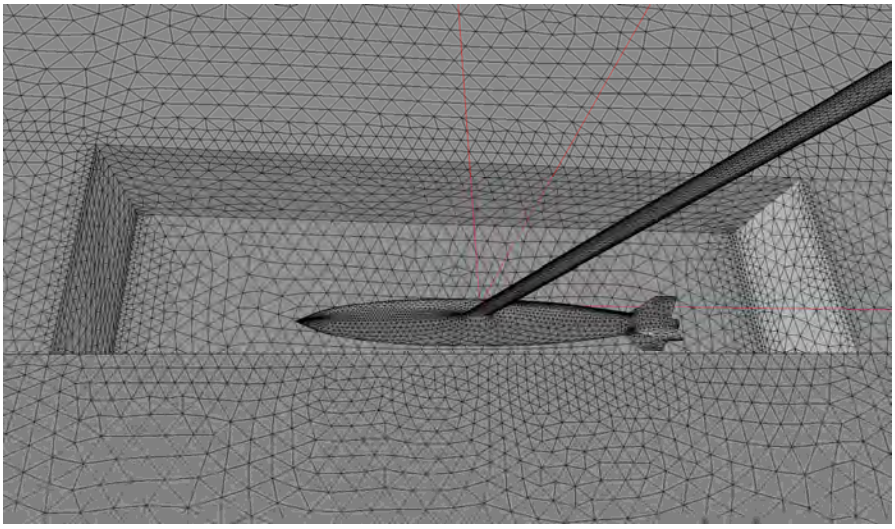

**Figure 8. Unstructured Cavity and Mk-82**

These unstructured grids are created from the point and line sources defined in GridTool. From the magnitude of these sources, VGRID solves a Poisson equation to establish the grid size at all locations on the surface. This process is equivalent to a solving a heat transfer equation, where the heat source are at different temperatures corresponding to the size of the placed sources, and the solution, or grid sizes, is representative of the temperature distribution across the surface.[5] The cells created from this solution are two dimensional, and generated sequentially on each patch, ideally equilateral, with some non-uniformity due to particular geometry allowed by the TetrUSS package. A completed surface grid can be seen in Figure 8, with a close up of the Mk-82 showing the distribution of cell size in Figure 9. It is important to note that a grid resulting in accurate simulation of the flow will have small cells at areas of radically different geometry and large cells in flatter regions. In this figure, the cells are very small at the nose and the edges of the fins, but large at the smooth areas on the side of the Mk-82 and larger still on the cavity wall.

[5] Frink, N., Pirzadeh, S., and Parikh, P., "The NASA Tetrahedral Unstructured Software System (TetrUSS)," ICAS Paper 0241, August 2000.

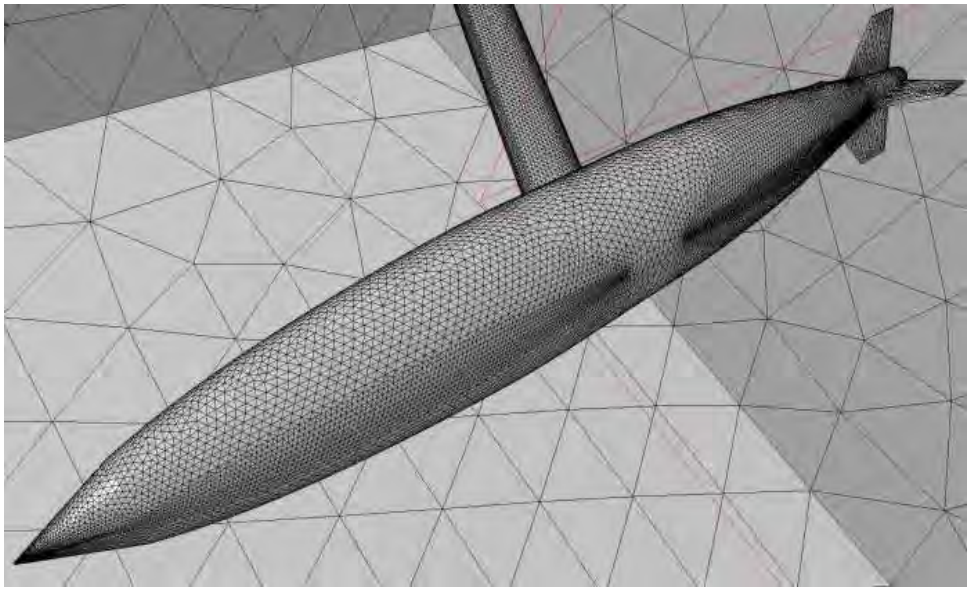

Figure 9. Mk-82 Surface Grid

**Table 2. Surface Grid Data**

| Model | Viscous Thickness (# of layers) | Viscous Cells (million) |
|---|---|---|
| Mk-82 | 25 | 5.04 |
| Mk-82 with strut | 25 | 5.25 |
| Cavity | 23 | 4.17 |
| Cavity with Mk-82 | 18 | 4.5 |

Generation of volume grids follows from surface grid definition, and is also accomplished using VGRID. In a viscous flow, the cell properties in the boundary layer close to the surface of the body change very rapidly, and as a result very thin cells are required in order to capture these rapid changes. In order to reduce the overall number of cells required, it is advantageous to keep these cells relatively large in all directions except that normal to the surface. In order to best produce this type of grid, the advancing layers method was developed. This method allows for the creation of relatively ordered cells while maintaining the flexibility of an unstructured grid, and has proven very successful in use. It was first developed and presented for CFD application by Shahyar Pirzadeh in 1993, and its method of propagation can be seen below in Figure 10.

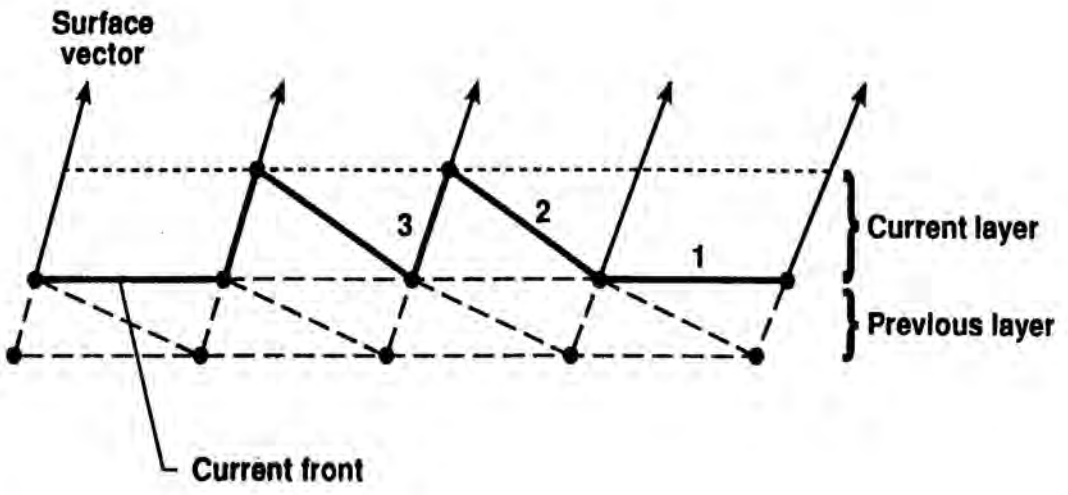


Figure 10. Advancing layers propagation method[6]

Beginning with the surface grid, a surface vector is created from each vertex pointing normal to the surface. The first layer of cells is generated by traveling a specified distance along each surface vector and essentially connecting the dots in the manner shown in the above figure. The first layer of volume cells is generated on each surface cell before the second layer begins, and the second layer is formed in the same manner as the first. The user can specify the initial height of the first cell as well as the rate of growth for the remainder of the layers, which allows great freedom in the number of cells created. It is important to note that this method operates independently of the background source grid; it propagates using only the spacing parameters specified. An example of the viscous layers generated on the Mk-82 can be seen below in Figure 11. The first layers are far too small to be noticed, but by the end of this method's propagation the layers are quite thick, as can easily be seen on the side of the store. Depending on the type of flow solver being used, this thin layer of cells can vary from just a few for an inviscid Euler flow solver to a hundred or more for a Navier-Stokes solution using a Spalart-Allmaras turbulence model. It is interesting to note that for a full viscous solution, as many as half of the volume grid points may lay in the boundary layer region.

[6] Pirzadeh, S., "Unstructured Viscous Grid Generation by Advancing-Front Method," NASA Contractor Report 191449, 1993.

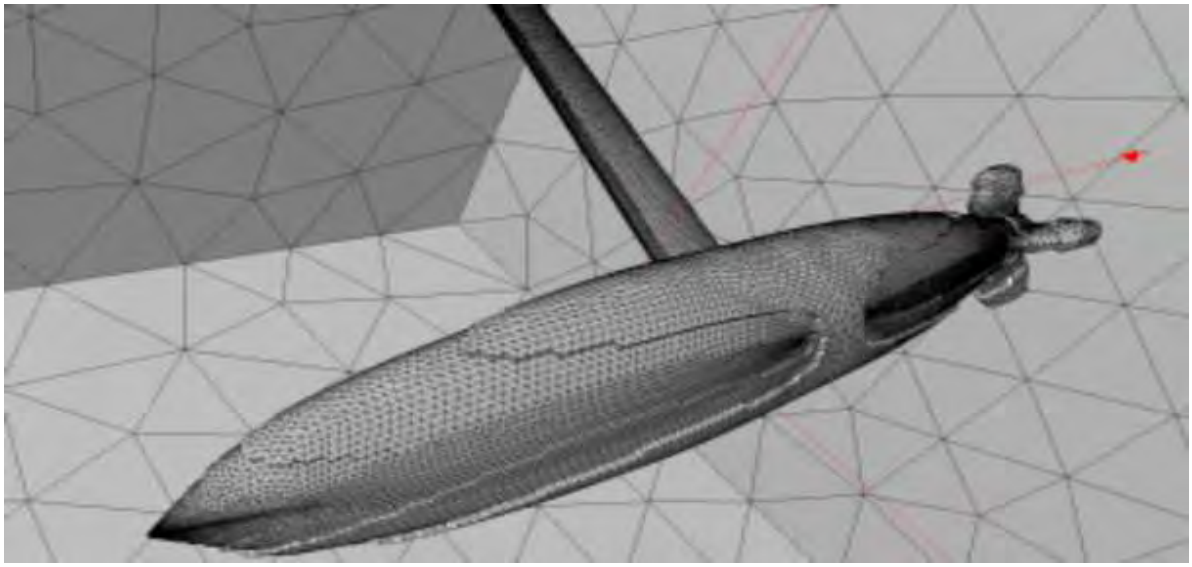

Figure 11. Viscous Layers on Mk-82

Once the region of the boundary layer is appropriately constructed using the Advancing Layer method, VGRID changes to an Advancing Front methodology to fill in the rest of the volume grid. This method is used for generating the inviscid portion of the grid, which comprises the large majority of the volume in any grid. In grids where viscous layers were generated with the advancing layers method, VGRID switches to the advancing front method when the volume of the next viscous cell would be greater than the background sources dictate the size should be. The advancing front method attempts to generate equilateral tetrahedra and therefore is not nearly as orderly as the advancing layers method, but has the advantage of greater flexibility which is necessary with complex geometries. Figure 12 shows a two-dimensional grid created with both methods, illustrating the point of transition.

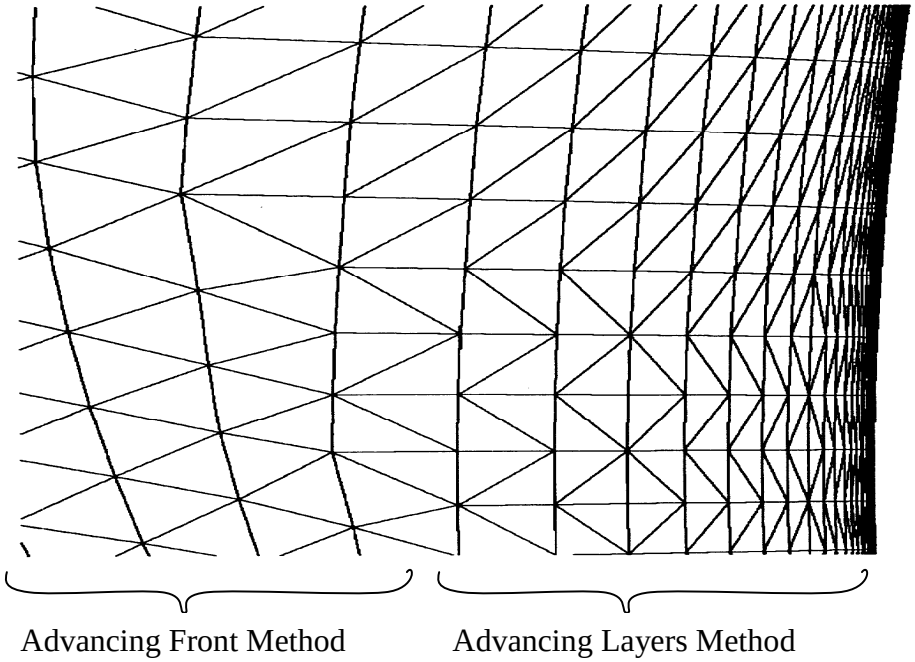


Figure 12. Two-dimensional grid using advancing front and advancing layers methods[7]

It should be mentioned that grid generation for CFD solutions is an iterative process. Properly accomplished, the process converges on a flow solution that can be used to provide a flight clearance for that release condition with a high degree of confidence. The cyclical process begins with geometry manipulation; then grid generation, followed by flow solution. A close analysis of the flow solution, or the flow solver's failure to converge on a solution typically reveal areas in the geometry manipulation and grid generation that need to be improved. This continues until the engineer is satisfied with the results, typically by validating CFD solutions along the way against existing measured data.

The advancing front method also propagates in a different manner. Instead of working layer by layer, it generates new cells along the current front. The current front is defined as the

[7] Pirzadeh, S., "Unstructured Viscous Grid Generation by Advancing-Front Method," NASA Contractor Report 191449, 1993.

boundary between the gridded and un-gridded regions, and is constantly changing as new cells are created.

Figure 13 below shows the generation of the volume grid by this method. The majority of grid growth begins at the sharp edges of the store, and continues in a somewhat spherical manner until the entire box is filled with cells.

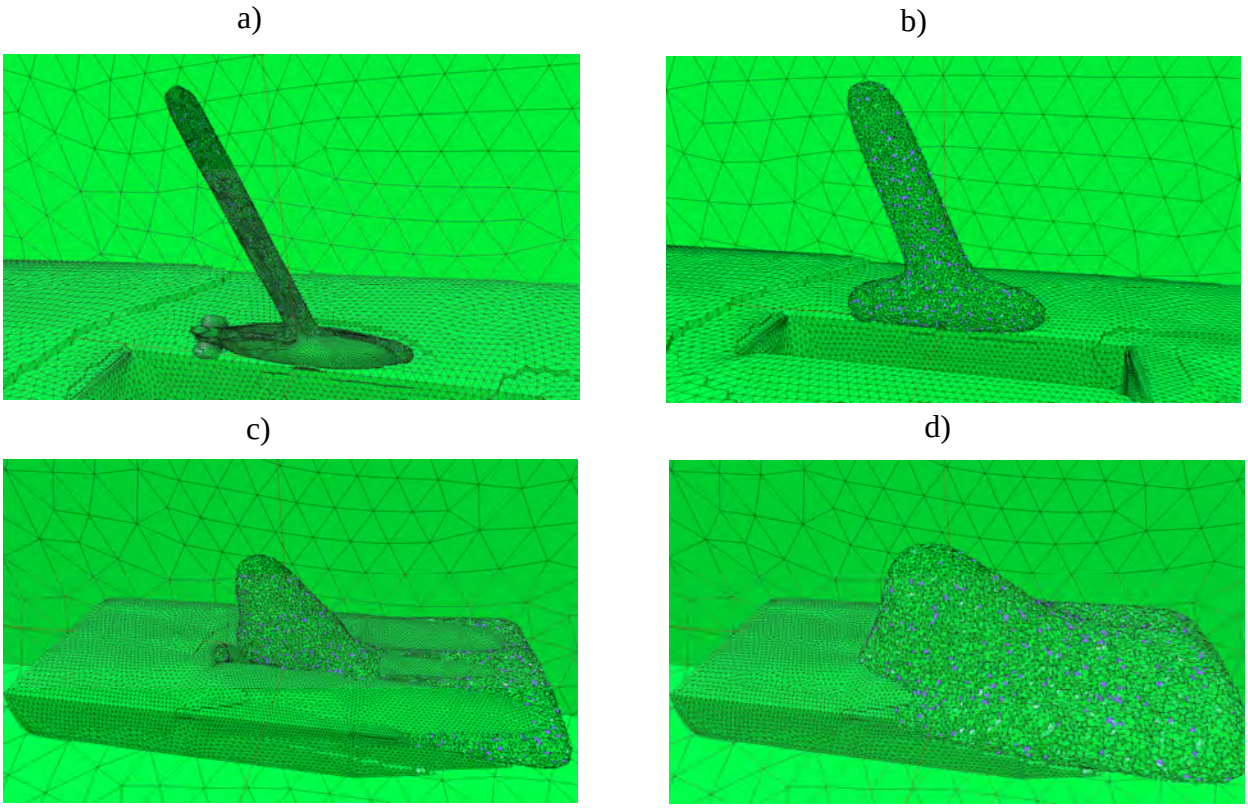


Figure 13. Generation of volume grid by advancing front method

Volume grids were generated in this manner for each configuration in this project, and the total number of cells produced in each can be seen below in Table 3.

**Table 3. Volume Grid Data**

| Model | # of Cells (million) | # of Nodes (thousand) |
|---|---|---|
| Mk-82 | 6.78 | 1105 |
| Mk-82 with strut | 7.20 | 1226 |
| Cavity | 2.21 | 387 |
| Cavity with Mk-82 | 5.63 | 958 |

## USM3D

Once the volume grids are generated, steady-state flow solutions were obtained using the USM3D flow solver, designed for use with unstructured grids. USM3D is a very flexible flow solver, featuring options for different types of flow, inclusion of jet engines or propellers, various face boundary conditions, and the ability to integrate flow properties on a specified set of surfaces, among many others. This last feature is especially important to this research as determination of the forces and moments on the store is the entire goal of CFD calculations. USM3D is a cell-centered solver, which requires fewer tetrahedra and therefore less computer memory relative to the node-centered method.[8] USM3D is also capable of multiple different types of flow simulations. It can perform pure inviscid calculations using Euler's formulation of the flow equations, pure laminar flow calculations, full viscous calculations using the Spalart-Allmaras (S-A) turbulence model, or viscous calculations using a wall function based on the S-A model. Flow separation is greatly dependent on turbulence modeling when using a full Navier-Stokes solution and good results have been found in the past using the Spalart-Allmaras turbulence model.

This research has employed the wall function method for multiple reasons. This method operates by applying an analytic function to the sub-layer portion of a turbulent boundary layer. This region would otherwise require many very thin cells in order to achieve accuracy, and the removal of these cells has the double benefit of greatly reducing the total number of cells in the grid and removing solution stiffness which is inherent in thin cells. See Frink[8] for more details on the operation of this method. Regions of the cavity have aft facing blunt surfaces which will obviously lead to flow separation inside the cavity. GridTool has engineering tools to specify various boundary conditions to the flow solver to capture the physical aspects of the problem. It is not obvious a priori which of these methods will yield the most accurate results hence the

[8] Frink, N., "Tetrahedral Unstructured Navier-Stokes Method for Turbulent Flows," AIAA Journal, Vol. 36, No. 11, November 1998, pp. 1975-1982.

importance of the measured test data in the form of the NICS wind tunnel study for validation purposes along the way

It is also important to note that flow solutions are not generated in a single step, they require numerous iterations to reach a steady solution, at which point the solution is said to be converged. This type of solution is known as time-marching, and is the result of the chosen numerical method to solve the Navier-Stokes equations. In CFD research convergence is typically evaluated using the concept of residuals, which measure the amount of variation in flow properties from one time step to the next. Experience has shown that solutions can be considered converged when this variation between times is 3-4 orders of magnitude smaller than the original change. In order to reach convergence, models have been run from 4000 to 12000 iterations. Due to the lengthy amounts of time required for a full solution, it is generally wise to examine the value of these residuals over time to ensure that they are decreasing and the solution is converging. Because of the highly separated flow around the cavity, a solution with a two order of magnitude residual drop was then evaluated for stability by examining the moment coefficients and their stability.

USM3D outputs a file at each time step which contains the value of the residuals and coefficient values. To facilitate this analysis, a program was written in MATLAB which reads the USM3D output file and graphically plots the logarithm of the decrease in residuals versus time. A screenshot of the interface for this program can be seen below in Figure 14. In addition to this, the values for the coefficients were plotted as can be seen in Figure 15.

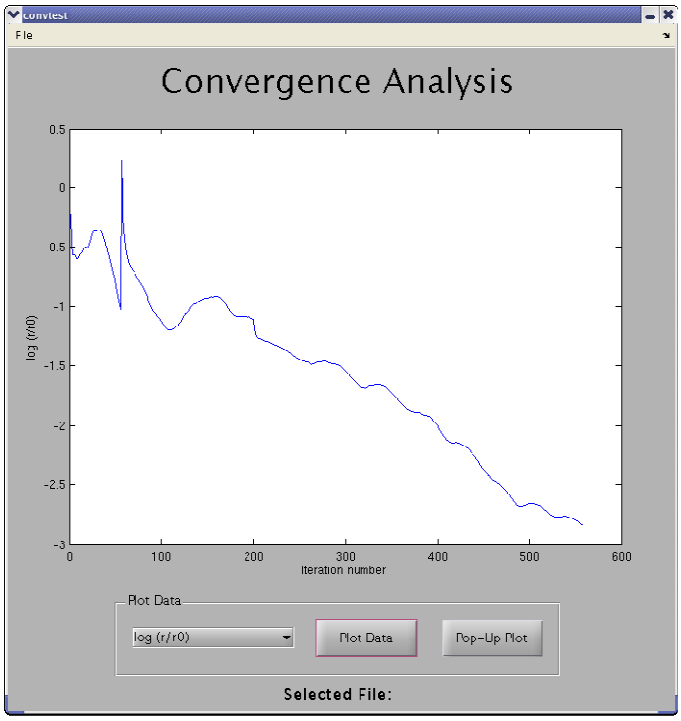


Figure 14. Screenshot of Convergence Analysis program

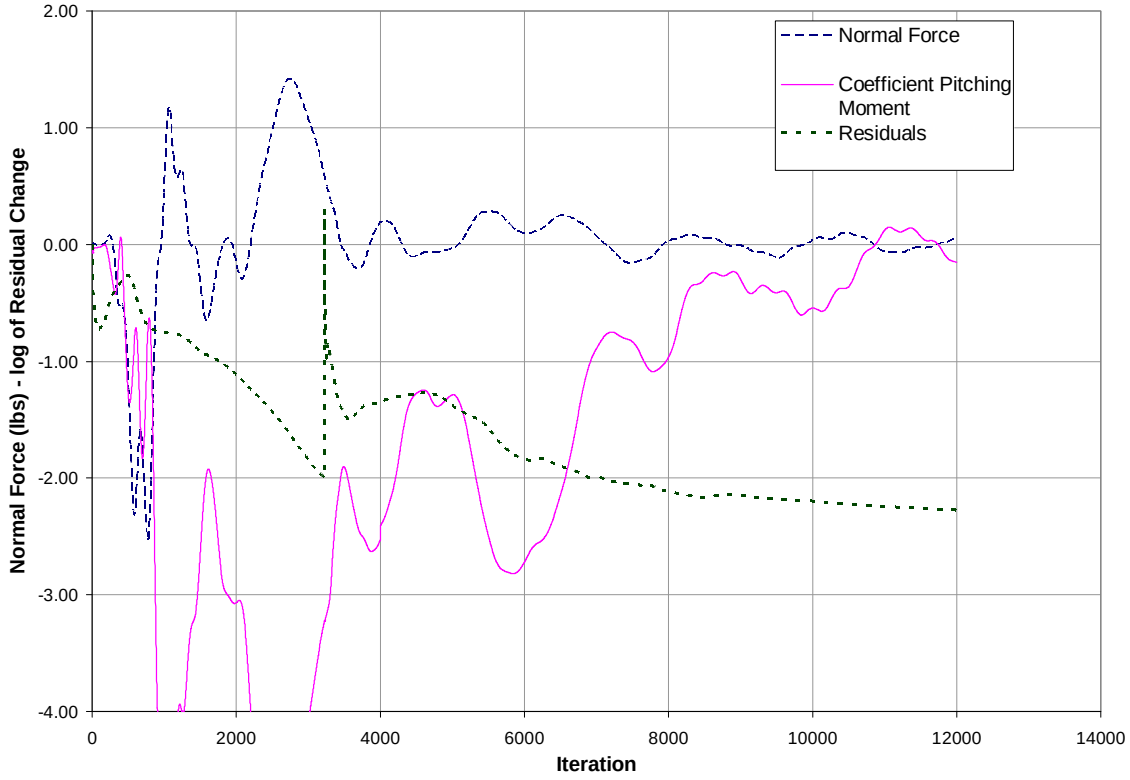


**Figure 15. Convergence Study**

The USM3D flow solver can be run using parallel processing on the Linux cluster in CADIG room of Rickover, allowing for solutions to be generated relatively quickly.

An auxiliary function of the USM3D code is an option named the "FandM" calculation. "FandM" stands for Forces and Moments, and is used to find the forces and moments upon specific pieces of the geometry while ignoring others. This was critical in the project, as the forces upon the modeled sting would have thrown off the results completely. In the NICS configuration, the sting was covered with a sheath that allowed the aerodynamic forces upon that structure to be ignored. In simulating that mechanical setup, including the protective sheath, the USM3D code would sum the forces and moments upon every patch except those which made up the sting. In this way, the forces upon the sting were ignored and the aerodynamic effects of the sting upon the forces of the tail and other surfaces were determined. This was an absolutely necessary function of USM3D, and serves to illustrate its versatility and usefulness.

## Flow solutions

The output of the USM3D program is the pressure distribution over all surfaces, which can be used to calculate lift, drag, and moments on any region, or sub-region of the geometry, i.e. the store alone, the cavity alone, etc. Figure 16 shows a pressure distribution solution found with USM3D and displayed with a commercial visualization product, TecPlot. TecPlot allowed for a display of large amounts of data in an elegant and easily understood manner. Pressure distributions, shock waves, streamlines and flowlines are just some of the methods for analysis that TecPlot supports. The entire grid file is loaded into TecPlot, showing the exact meshing that was analyzed by the TetrUSS package. Selections can be made to show the entire volume, or the surface of the object.

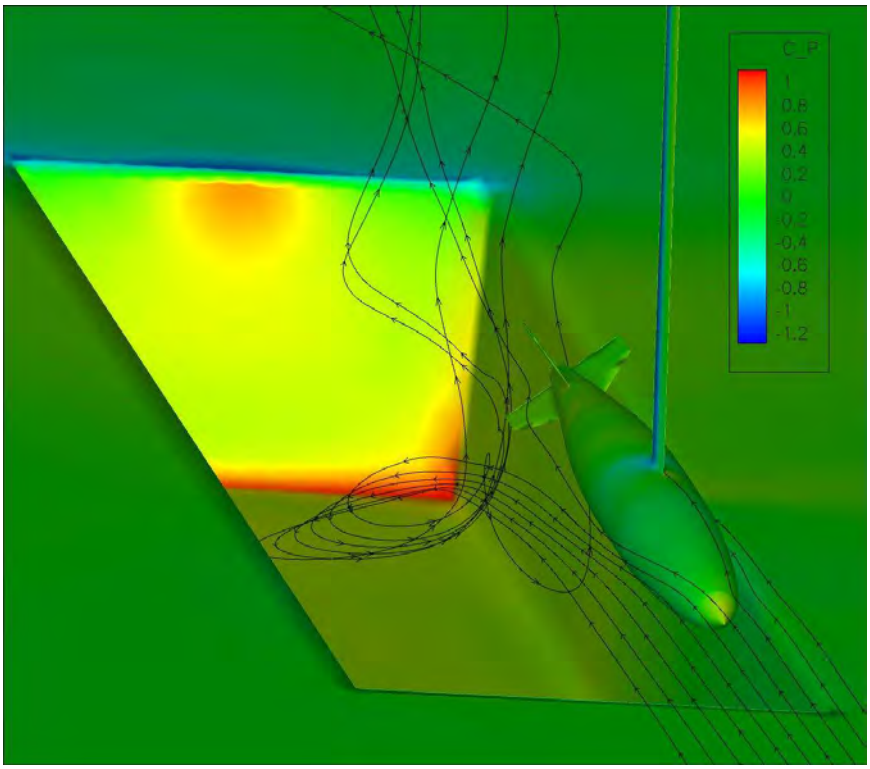


**Figure 16. Pressure Distribution of Cavity and Store generated with USM3D**

The quantity represented by the colors on the plane's surface is C_P ( $C_p$ ) instead of actual pressure. $C_p$ represents the pressure coefficient, and is the standard way to non-dimensionalize pressure. The pressure coefficient is defined as follows:

$$C_P = \frac{p - p_\infty}{q_\infty}$$ Equation 5

where $p$ is the static pressure at the point of interest, $p_\infty$ is the freestream static pressure, which is a function of altitude, and $q_\infty$ is the freestream dynamic pressure, which is a function of the ambient density and the velocity of the aircraft. This coefficient allows tests made at different altitudes or airspeeds to be compared to one another. As expected a good portion of the cavity is green, meaning these regions have a pressure coefficient near zero and a static pressure equal to ambient pressure. Areas where the flow essentially stops or stagnates, such as the nose of the store and the front of the cavity, have a high pressure coefficient and therefore a high static pressure. The areas around the edges of the cavity, particularly the back corner, have static pressures below that of the ambient flow and thus have negative $C_p$ values. The static pressure distribution along a surface of a shape can be integrated to find the resulting force and moment on the shape due to the flow.

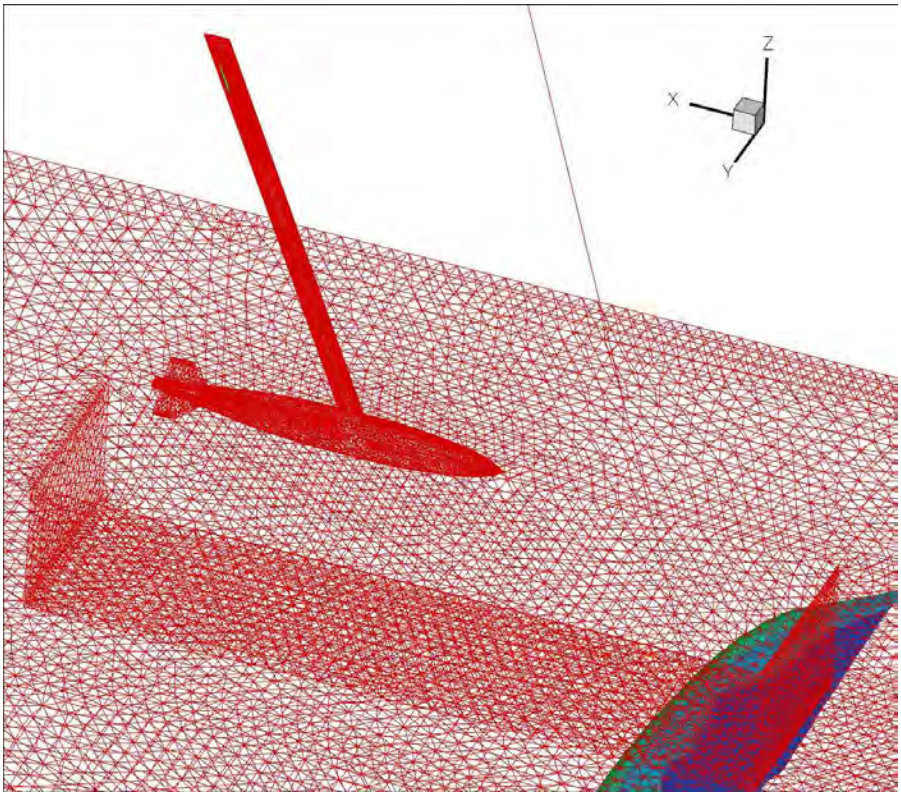


**Figure 17. Shock Wave Analysis**

The model and configurations were analyzed for the potential of shock waves. With a freestream velocity of Mach 0.85, there existed the potential for a Mach wave to form, thus creating a very different flow pattern and interfering with the data. This is one of the benefits of CFD, where you can analyze every portion of the structure and airflow, as compared to the wind tunnel, where there is one chance to gather your requested data. Figure 17 shows the TecPlot view of the surface mesh of the cavity and the store in red. The blue and green blob in the lower right hand corner is the appearance of a shock wave on the other side of the model. As can be seen in Figure 5, the bottom of the cavity housing is angled sharply. At that angle, the airflow changes directions rapidly enough to produce a shock wave. The only other place that such a shock is formed is on the side of the sting at the very tip, furthest from the store. It can be seen in Figure 17. As the forces upon the sting were not measured, this shock does not create an issue for the analysis of the data.

# DEVELOPMENT OF ANALYSIS

## Test Matrix

Eight different configurations were generated corresponding to the store in one of seven possible longitudinal locations along a traverse at the opening of the bay, plus an empty bay configuration. The range of configurations is shown in Figure 18. The grid sizes were determined through a refinement process explained in the following section with the resulting volume grid containing approximately 20 thin layers near the surfaces of the geometry (viscous region) and a final tetrahedral count of approximately 6 million for the complete grid. The USM3D flow solver was run until the log of the residuals had dropped approximately two and one half orders of magnitude and the forces on the store had generally stabilized. Since it is known that the flow is actually unsteady in the bay, it was anticipated that this convergence of this steady-state solution would not be as good as for an external/pylon configuration. However, the study was trying to determine the degree to which the flow in the vicinity of the store at the opening of the bay is steady and how closely these computations would match results from the wind tunnel test, also a time-averaged steady state phenomenon due to the mechanisms of the sting measurement apparatus.

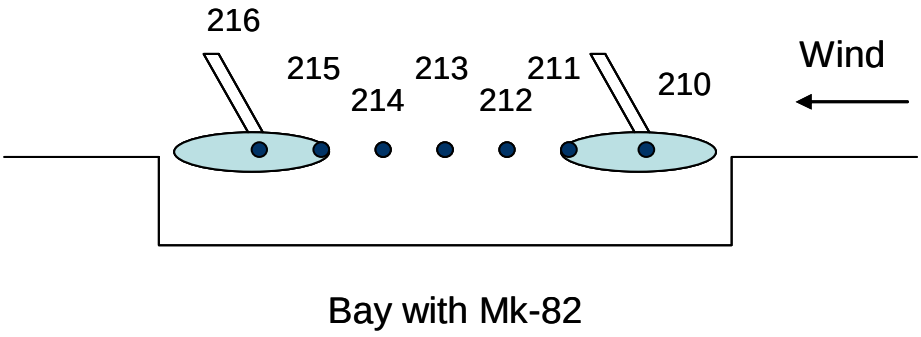


**Figure 18. Test Matrix for CFD comparison to NICS data**

### Forces and Moments

Once the generated data is post-processed, the pressure distribution on the Mk-82 will be used to determine the direction and magnitude of the aerodynamic forces acting on it. When compared with the forces generated on the Mk-82 in freestream conditions (without an aircraft nearby), a set of aerodynamic influence coefficients can be developed. By running multiple tests with the stores at many different positions within the cavity, a grid of influence coefficients can be generated that depend on spatial position. It is felt that these coefficients, which are also available at certain discrete points from the wind tunnel tests, are the metric that need to be evaluated or matched in order to compare a computational flow solution to experimental results. Since these coefficients reflect the influence of the shear layer on the store, a close match should indicate that the flow solution generated by CFD is indeed a good representation of the actual flow. Advanced visualization techniques on the CFD flow solution can be used to study the behavior of the shear layer.

It is also possible to use the USM3D flow solver to compute the time-accurate flow over a geometry. When the flow is steady, this method should converge to the solution previously addressed. In the case of large areas of flow separation, the flow may not be steady. In that case, the force on the store in the unsteady flow will fluctuate. It is hypothesized that the mean value of this fluctuation should match measured wind tunnel data since the wind tunnel returns time averaged load data. Furthermore, it is thought that an analysis of the fluctuations can be used to bracket the ‘unsteadiness’ in the flow, at least in terms of its effect on the store. This bracketing will have a role to play in a parametric analysis of the stores trajectory.

### Trajectory Simulation

There are two standard approaches used to apply CFD to the prediction of store trajectories. The first, known as moving/time-accurate, incorporates a six-degree-of freedom module (6DOF) with the flow solver code. The flow solver first solves for the pressures at all points on the store, and using these it determines applied forces. These forces are then sent to the 6DOF, which determines how far the store will move over a specific small time step, and the new position is sent back to the flow solver which computes the aerodynamic forces at the new

position. With enough iterations an accurate solution can be obtained. While the term, time-accurate, is applied to this method, it should be understood that this applies to the generation of the store trajectory as well as the computations of the flow solver. This method typically requires complex moving grids utilizing a grid interpolation scheme sometimes called a chimera approach and is extremely computationally expensive. It produces one trajectory as a solution, and if any variable is later changed, the whole process must be repeated to obtain a new trajectory.

The other method, known as the grid method, allows more flexibility to the engineer. It often requires more computational time up front as flow solutions at numerous points on the flow need to be calculated, but can be far more computationally efficient if parametric analysis of the release condition is to be performed later. The grid method essentially assumes that the flow is quasi-steady, although various techniques can be used to capture the effect of unsteadiness in the flow. This is the method that was used in the research test here. It is based on tests of the store in various positions and orientations in the cavity to create a grid of aerodynamic influence coefficients. When these coefficients were determined over a range of positions, they were input into the Navy Generalized Separation Package (NAVSEP).

Generated by the Navy to ensure safe store separation, this program will combine the aerodynamic influence coefficients generated by TetrUSS with free-stream data and other forces such as gravity, ejectors, and attachment points, applied to the stores. Figure 19 is a graphical representation of the myriad of inputs that go into the NAVSEP program. Beginning from the left side of the graphic, the grid totals are found through either the CFD analysis, here calculated by the FandM function described in the USM3D section. Another way to find these grid totals is through CTS, the captive trajectory system. This sting moves the store to pre-determined locations and measures the forces and moments. AEDC did this with the NICS data set, which was used to compare to the answers from CFD. Those numbers are then manipulated by the free-stream values that were calculated using each respective method. The free-stream forces are subtracted from the total grid forces to create grid coefficients, the change in force between that position and the free-stream values. NAVSEP, the 6DOF program, accepts these coefficients. In order to scale the forces, the right side of the graphic shows the large or scaled free-stream data.

This is used to convert those coefficients from the left side into actual forces and moments. Information, such as the moments of inertia, the desired resolution, and the forces and geometry of the ejector forces are supplied to the program in the form of a large input file. It rapidly interpolates, and writes a complete file detailing how the store will fall given the inputs. For other trajectories, it is easy to change a piece of information and re-calculate, analyzing a large number of trajectories.

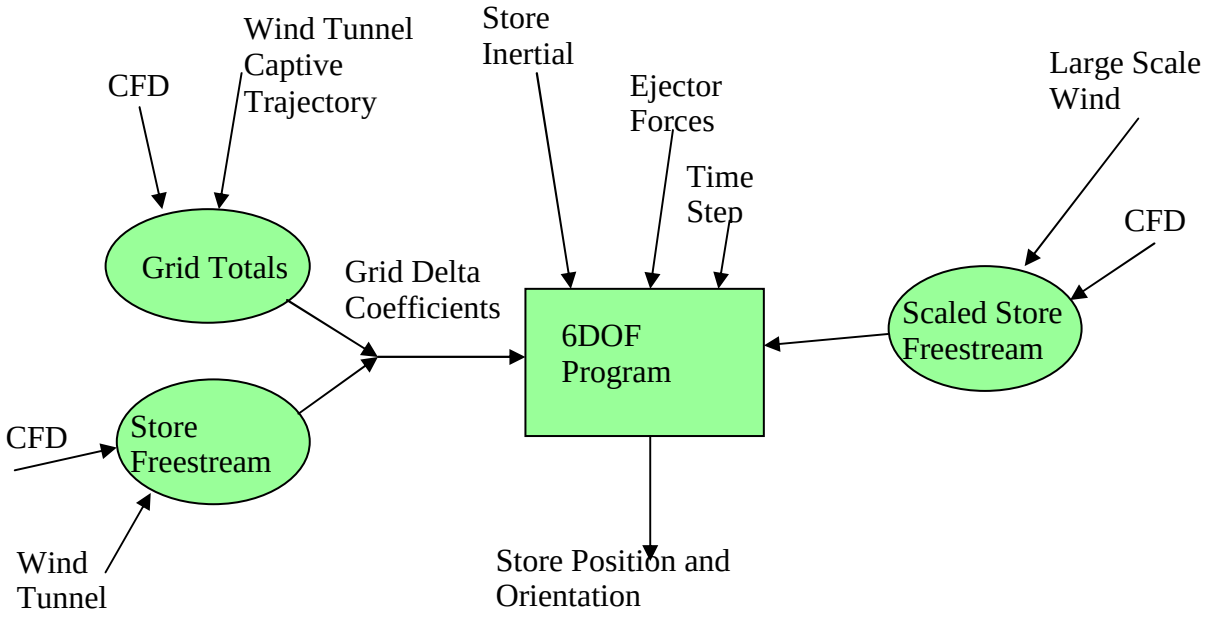


**Figure 19. NAVSEP Inputs for Grid Method**

The freestream aerodynamic data needed will be obtained from both CFD and wind tunnel testing to verify accuracy and convergence on the same values. Large scale wind tunnel results are preferred and are available for the Mark 82. Using a built-in 6DOF (six degrees of freedom) calculator and time-step ability, NAVSEP will calculate the total force exerted on the store, determine the acceleration created by that force, and apply that acceleration over a very small time interval. It will then recalculate the acceleration at the next position, accounting for the velocity generated by the acceleration at the previous location. Using a very small time interval, an accurate trajectory can be calculated. Data generated from the time accurate CFD calculations can also serve to bound the magnitude of the influence coefficients. With appropriate bounds in place, initial release conditions, notably store mass and ejector force, can be varied in a parametric fashion in order to provide a family of possible trajectories.

The CFD data that was the input to the NAVSEP program had to be modified slightly in order to provide accurate trajectories. Because the vertical traverse at position 216 had not extended beyond the influence of the cavity, the interpolation of the program interpreted the numbers as a steadily increasing force or moment. Therefore the trajectory changed in many ways it should not have; instead of exhibiting stable traits, such as returning towards 0 degrees of yaw angle after a brief departure, the store would continue to increase that angle. Therefore, a freestream data point was added to the CFD data set, a point far away from the cavity with the moment coefficients set equal to 0, equivalently a dummy point to force the return to equilibrium.

Analysis of the trajectory solutions will be used to derive engineering metrics for store separation that relate store mass, ejector force, and flow unsteadiness to variations that can be expected in the resulting store trajectory simulations. A benefit of this method is that the same grid can be used many times with different initial positions and ejector forces in a parametric fashion, or elements of the grid can be varied during the trajectory calculation to bound worst-case trajectories for the store.

# RESULTS

A systematic approach has been used throughout this research project in order to produce accurate and replicable data. The first phase consisted of validation of the geometric models used for the wind tunnel replication. Once the models were validated, the configurations as specified in the test matrix description in the previous section were created using a utility program in the TetrUSS package. The flow around these configurations was calculated to convergence and the forces compared with the wind tunnel data. Once the longitudinal traverse was calculated, two different vertical traverses were studied. One was placed at the mid-point of the cavity, while the other was at the aft-most position. Additionally, a grid refinement study was done in order to ascertain the grid created was sufficiently complex. Once the forces and moments were calculated, the values were put into the 6DOF program along with specified conditions and several trajectories were predicted using the CFD data and the wind tunnel data from the NICS. These trajectories were then compared to validate the CFD analysis of this complex problem.

## Mk 82 Model Validation

One of the difficulties in conducting a store separation from a cavity test in a wind tunnel is the engineering of the sting apparatus to support the store and measure the store loads. For external applications, the sting is mounted in the tail of the store where its effect on the flow is minimized. For the NICS tests, the sting used a faired pylon mounting. Wind tunnel data for the store and sting in the free-stream indicated that this configuration had an undesirable influence on the store loads at positive angles-of-attack in excess of ten degrees. In order to verify the geometry of the store used in the CFD study, an angle of attack sweep of the store in free-stream conditions was performed. The Mk-82 with the sting modeled was run at 20 different angles of attack, from -20 to 20 degrees by 2 degree increments. The Mk-82 without the strut, or the “clean” model, was tested at 10 configurations, from 0 to 20 degrees by 2 degree increments.

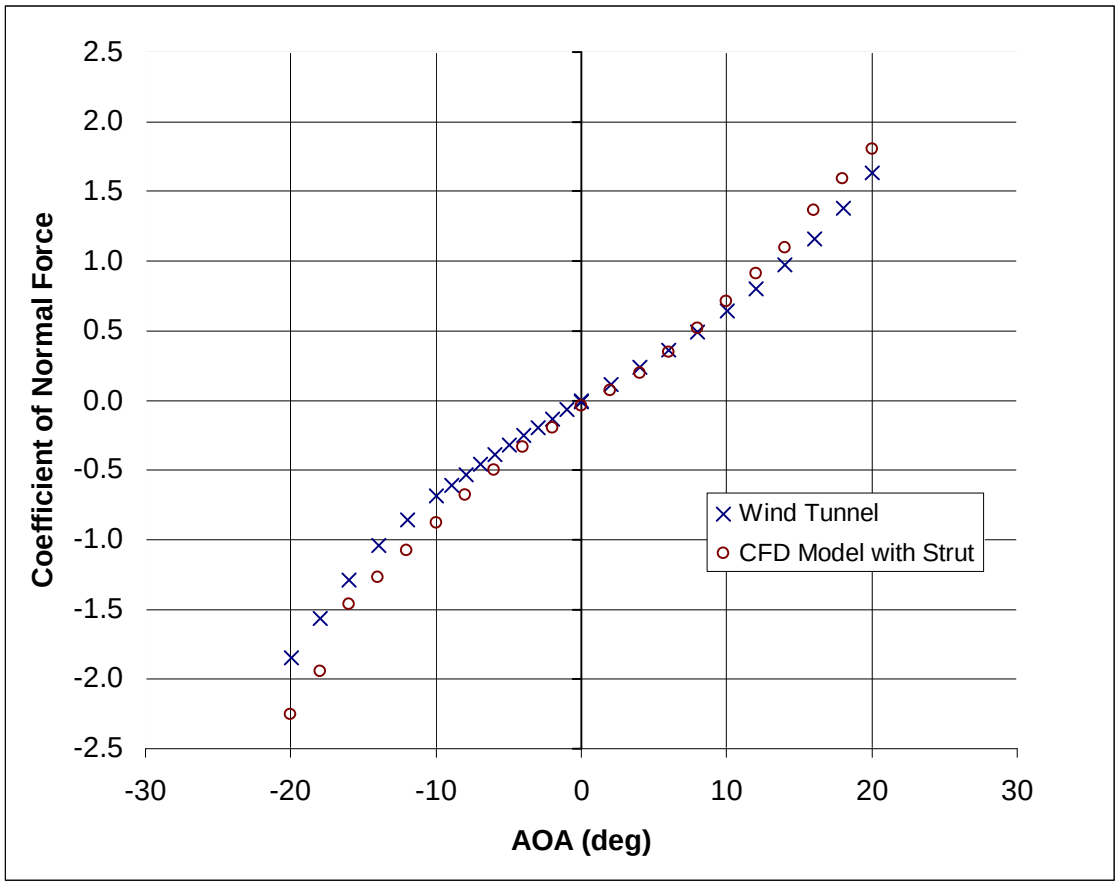


**Figure 20. Normal Force Comparison**

The normal force comparison provided a good match for the free-stream tests of the store without the pylon mounted strut. Tests were then conducted on the configuration with the strut. The pitching moment comparison for positive angles of attack, which is where discrepancies were largest, is shown in Figure 22. The data indicates that CFD modeling of the strut did not fully capture the effects of the strut on the flow in the wind tunnel tests. Conversations with the lead engineer at the original NICS tests indicated that the discrepancy may lie in the CFD not fully modeling the sting apparatus below the strut assembly, or perhaps in changes in the roundness of the leading and/or trailing edges of the faired strut in CFD from the as-built geometry although the latter difference was not felt to likely be the cause.

Unfortunately, no records of the exact geometry of the strut assembly remain from the NICS test although the lead engineer did indicate that he wished he had known that it probably was not the faired strut causing the discrepancy and some other piece of the apparatus at the time of the test. CFD results indicate that strut effects account for about $1/5^{th}$ of the influence of the

sting apparatus with the remaining difference arising from something else. This study decided to continue with the strut as modeled as results were in very good agreement for pitching moments at negative angle of attack, seen in Figure 21. This corresponds to the store pitching away from the opening of the bay which is the direction that the NICS testing showed. In addition, it is important to mention here that it is not anticipated the store will see above 10 degrees of angle of attack with the relative wind in the bay, although it is a possibility. At high positive angles of attack, convergence could not be reached, most likely due to high levels of separation from the sting, creating a condition unsolvable by the numerical approximations. A more in-depth study of the sting and potential shapes to mitigate the effects could greatly aid in obtaining accurate data.

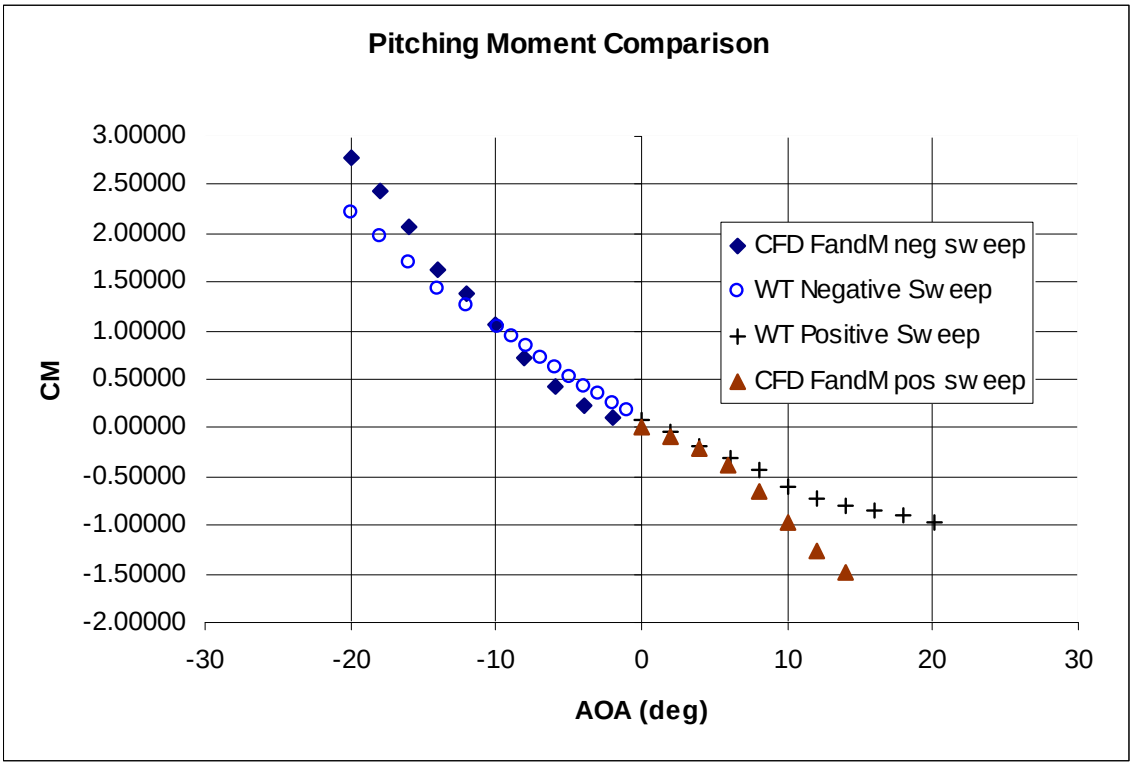


**Figure 21. Pitching Moment Comparison**

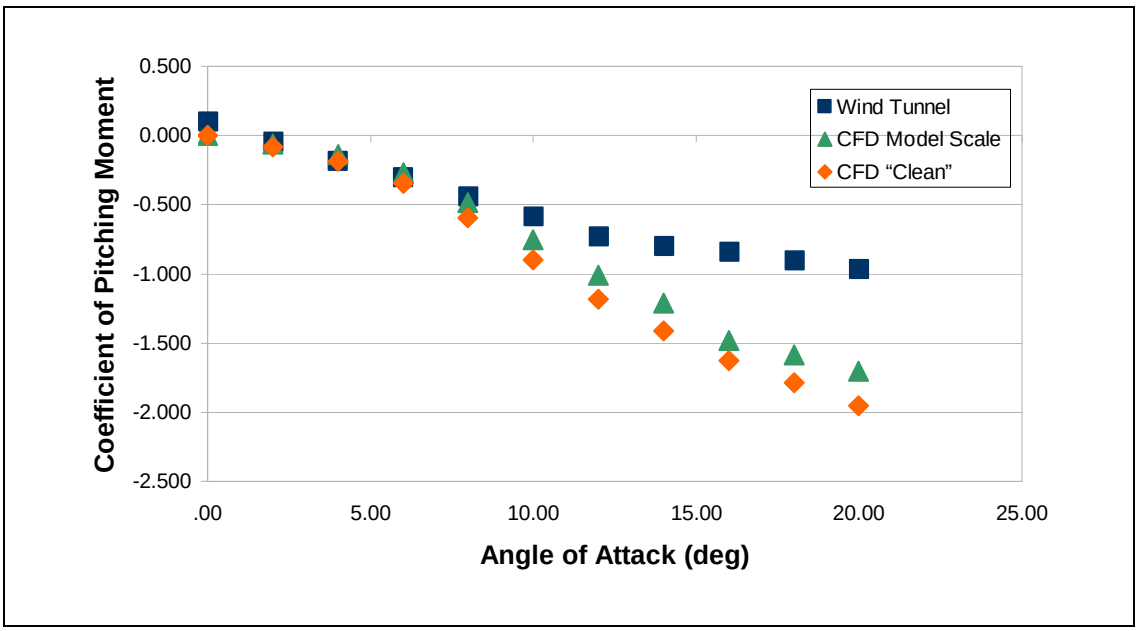


**Figure 22. Strut Effect Comparison**

The strut effect discussed above can be seen in Figure 23 as well, although not as significantly. The fact that it does not affect the coefficient of normal force as strongly is indicative that the strut effect is complex and does need to be studied more.

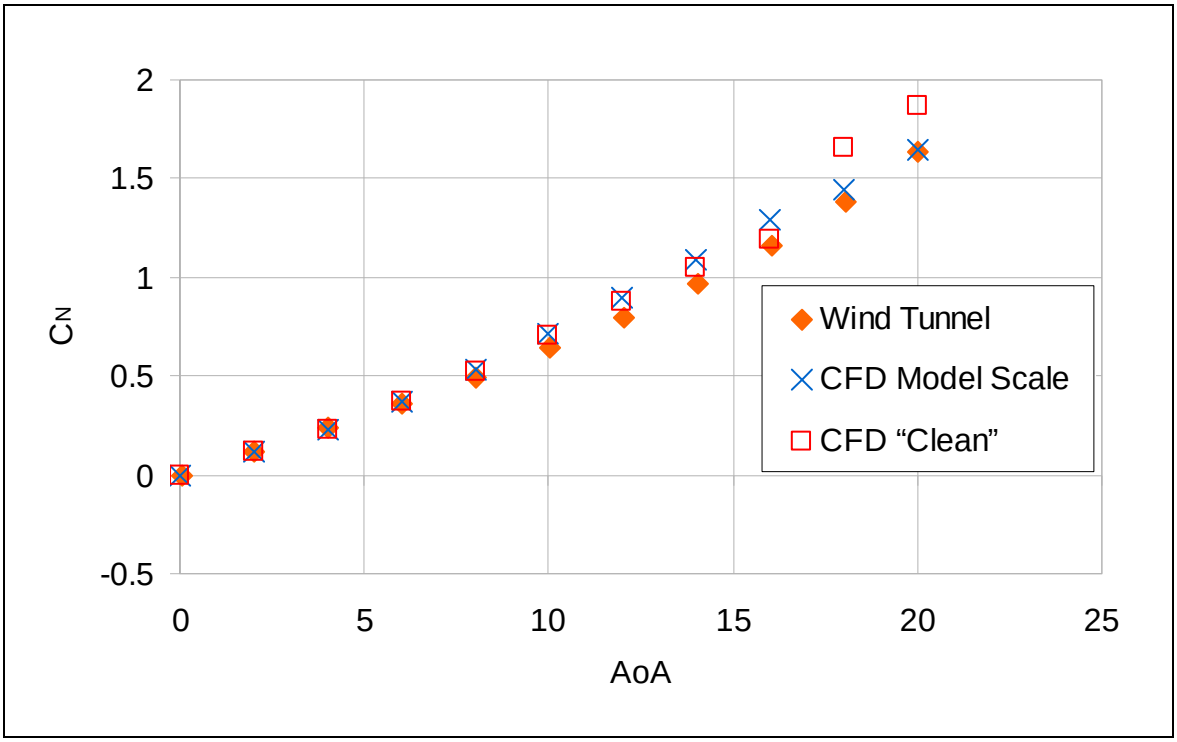


**Figure 23. Comparison of Normal Force**

## Characterization of Shear Layer

In order to test the shear layer behavior in an empty cavity, Tecplot was used to show the streamlines of the airflow across the mouth of the cavity, as shown in Figure 24.

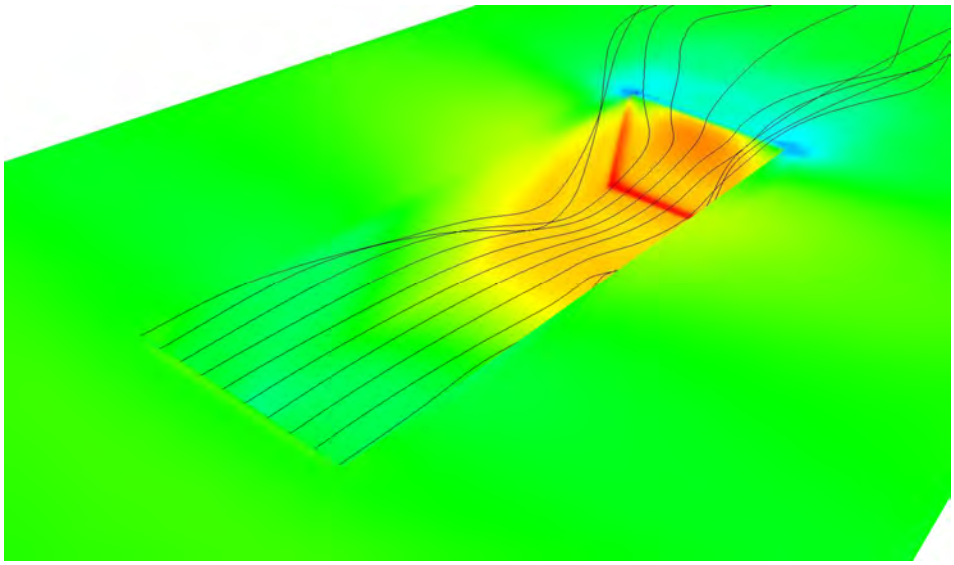

**Figure 24. Flow Visualization of the Empty Bay from CFD**

The flow visualization for the airflow around the Mk-82 when in the cavity was produced in order to compare the effects of the Mk-82 on the shear layer flow. Figure 24 shows the depth to which the shear layer dips into the cavity. The colors indicate the pressure distribution upon the surface. As expected, the corners of the cavity wall show the greatest pressure in this flow. Through the pressure plots and the streamlines, the effect the store has upon the flow can be understood more fully and therefore, make conclusions about the impact of different positions upon the store-shear layer interaction. This characterization was continued in the analysis of the vertical traverse effects upon the shear layer.

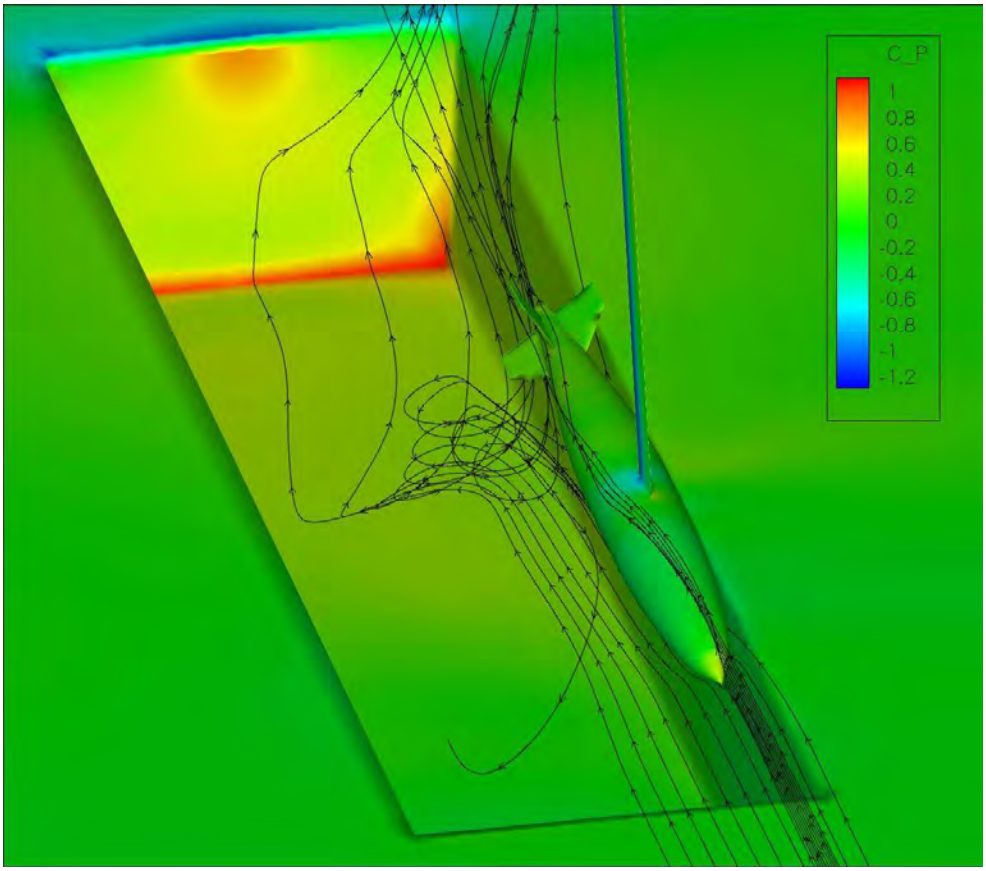


**Figure 25. Flow Visualization of Cavity with Store from CFD**

As can be seen through the previous figures, different positions within the cavity result in widely different airflow around the store and out of the back of the cavity. Figure 25 shows the streamlines around the flow swirling, then twisting around and out of the cavity, very different

from the flow as seen in Figure 26, even if the streamlines are located at the same beginning point. Figure 26 shows an interesting side to the expected high pressure areas and unruly streamlines. The flow clearly demonstrates that it does not dip nearly as deep as when there is no store in the cavity. At this mid-cavity position, just below the shear layer, the shear layer behaves quite differently than was expected.

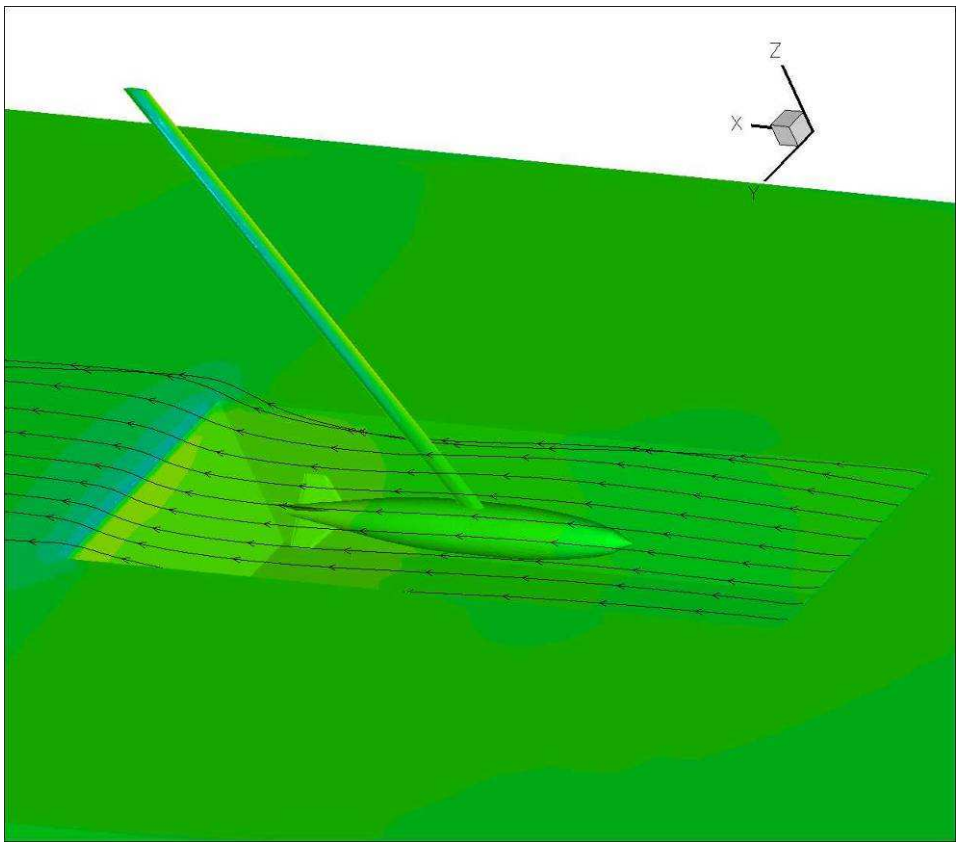


**Figure 26. Store Below the Shear Layer Visualization**

### *Grid Refinement Study*

A grid refinement assessment was performed with increasingly fine grids beginning at approximately 2 million tetrahedral and ending at approximately 10 million tetrahedral to verify that a sufficiently fine grid was being used. All grid sizes yielded approximately the same trends on the store and a grid size of approximately 4 million was selected as a good balance of computational time and flow resolution.

## Wind Tunnel Configuration

Using the geometry developed to replicate the NICS wind tunnel tests as closely as possible, CFD solutions were run on the bay with the store in one of each of the locations shown earlier in Figure 18. This corresponded exactly with the longitudinal traverse done in the wind tunnel tests previously. The center of the bomb was in line with the opening of the cavity, placing the store halfway in the cavity, halfway in the shear layer and the bomb was evenly spaced between the forward edge of the cavity and the aft-most. It was felt that at this position, the best values to characterize the shear layer would be found. The convergence history for one configuration located mid-cavity and labeled as number 213 is shown in Figure 27. The log of the residuals drops 2.25 orders of magnitude. The ripple in the normal force coefficient is much less than the ripple in the pitching moment coefficient on the store which was to be expected. The decision was made to stop the iterations at 12000. It was felt that further iterations would only diminish the ripple's magnitude slightly and not contribute to improving the accuracy of the solution. Further investigation into this problem and the nature of convergence would be significant in evaluating the limits of accuracy for the given approximations. An important fact shown by Figure 27 is the leveling out of the residuals right after 2 orders of magnitude lower than when it started.

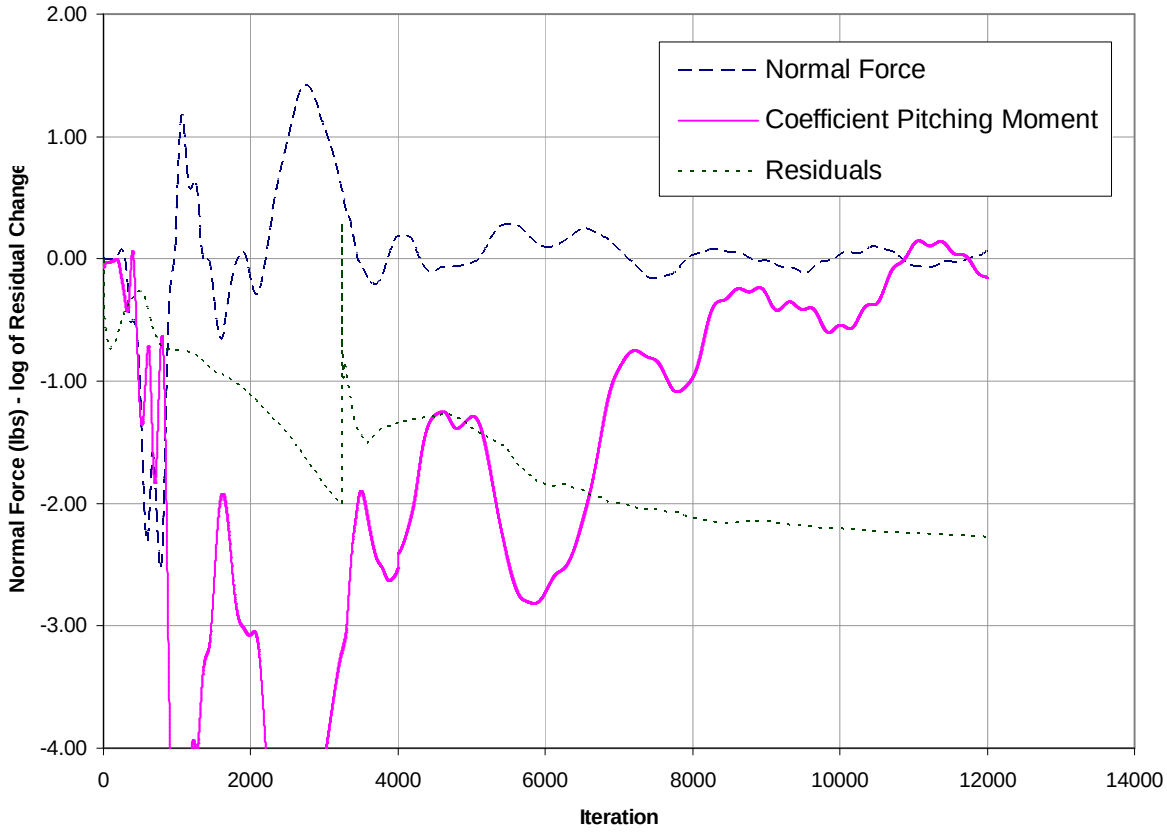


**Figure 27. Traverse Result**

An average value of the force and moment coefficients over the last 3000 iterations was selected as the basis of comparison for all configurations. This selection was made based upon the initial flutter, which began around 9000 and showed a repetitive wave in the magnitude of the normal force. As this was also the case for the pitching moment, the 3000 iteration mark was selected to capture both the average value as well as the standard deviation for evaluation against the wind tunnel values. Averaged forces and moments might seem to be neglecting the precise measurement one would expect of computational fluid dynamics calculations, however the wind tunnel also averages the forces upon the store in order to display a value. You could be reminded that this CFD solution actually represents the flow at a split second in time, and in an unsteady problem, convergence is not expected. The simple fact that the residuals dropped so significantly is tremendous. Somehow it is closing in on a steady-state approximation of the unsteady forces.

The ripple could be the flow bouncing between two steady state answers, without enough fidelity to converge on one or the other. This is no different from the averaging of CFD values in order to present a singular representation of that flow solution. The averaged CFD values will serve as our semi-steady state answer for lack of a completely converged answer.

### Longitudinal Traverse

The objective of testing the longitudinal traverse was to characterize the shear layer. If the S-A turbulence model could not handle the semi-steady flow, the data would show that. If the unsteady flow over the cavity and store was too complex and couldn't come close to being modeled, the CFD forces would be very different from those obtained in the wind tunnel. Once the comparison is made, a quantification of the feasibility of using CFD for solutions involving cavity store separation can be calculated. From this quantification, further studies can look at the feasibility of other approximation methods capturing more accurately this unsteady flow in a semi-steady state.

The solutions were obtained using the USM3D flow solver along with the "FandM" utility. Figure 28 shows the history of one of the most volatile coefficients, and the most critical in this study, the pitching moment. As expected, initially the values jump high and low, but the close nature of their paths indicates that the flow around the different configurations is not completely different. The high's and low's are paralleled across the 7 positions, but they don't begin to flat line or converge on a single value. The solutions were originally run out to 8000, at which point the values are scattered across the graph, and not resulting in any meaningful values. It was decided to run these configurations for an additional four thousand iterations, as some progress had to be made, and the residual count was decreasing steadily, indicating a move towards convergence. The 'ripple' at the end of the iterations can be seen, the jagged curves which hover around the range for reasonable values. Along with the average of the last 3000 iterations, the standard deviation was calculated in order to measure the level of ripple that was present in each of the configuration solutions. This value could be correlated to the level of activity of the shear layer, aiding in the characterization of the flow.

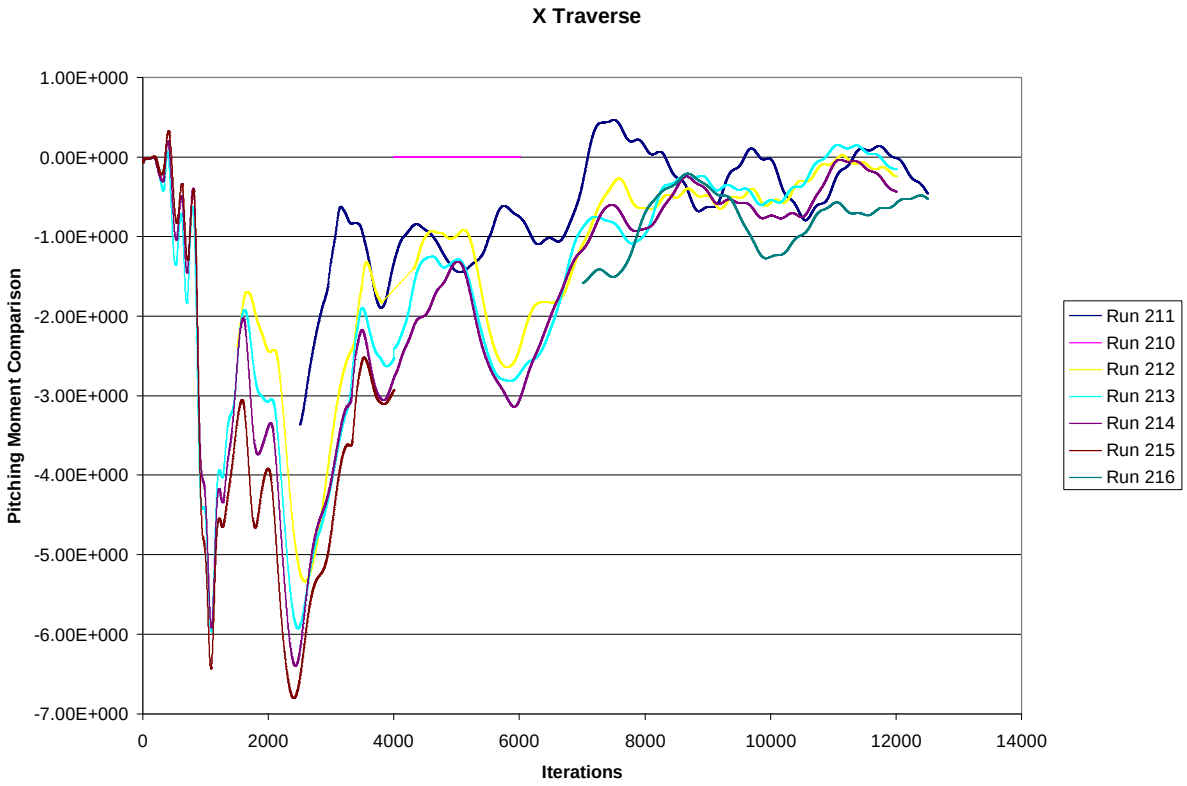


**Figure 28. Complete Iteration of Pitching Moment for Longitudinal Traverse**

The result for the pitching moment, which is the primary motion of interest in the store release, is shown in Figure 29. The agreement to the wind tunnel tests is generally good with CFD capturing the general trend in increasing the pitching moment on the store as the store is moved aft along the opening of the bay. CFD is under predicting the magnitude of the pitching moment by about 50% which is significant. Whether this is a result of the flow solution not fully converging or the inability of CFD to accurately predict cavity flow is a determination that could made given further iterations and more detailed study. The error bars demonstrate the range of the ripple by showing one standard deviation above and below the average value. While the prediction does not match well for the mid-range positions, at the front and aft of the cavity, the wind tunnel data is within that upper standard deviation of the CFD data. The trends shown by the wind tunnel are matched, a gradual increase in the pitching moment as the store moves aft. These results would suggest that the greatest uncertainty in the shear layer characterization is actually in the middle of the cavity, not the rear as some have thought. If this midpoint section of

the cavity is the furthest away from the semi-steady state calculations, the flow must be the furthest from a steady state flow.

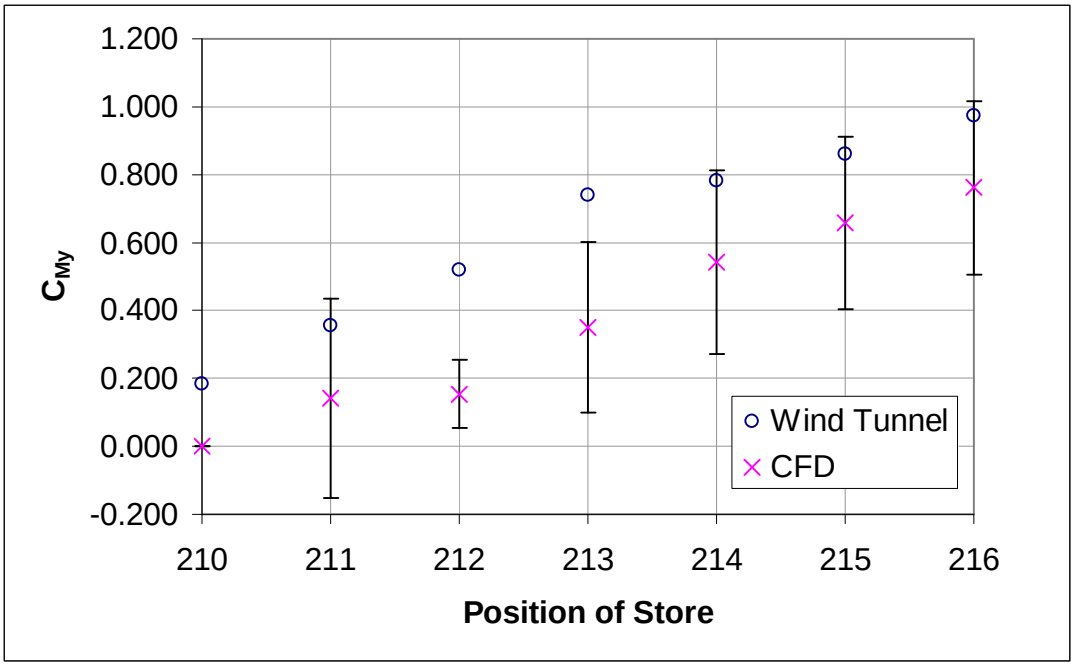


**Figure 29. Longitudinal Traverse Comparison**

### Vertical Traverse

Forces and moments on the store at various heights were calculated to provide the 6DOF solver, NAVSEP, with the information needed to calculate a trajectory. To make a complete grid of vertical traverses from each longitudinal point would have been overly time consuming. The position with the largest moments was chosen in order to capture the worst-case scenario. By evaluating this position, it can be assumed the store will not surpass the displacement shown at this position in the x-y plane. As seen in Figure 29, the position with the largest pitching moment is the aft-most: 216. In addition to this location, an additional vertical traverse was studied at the mid-cavity position: 213. This provided another group of data with which to characterize the shear layer at that point. Figure 30 shows a visual representation of the vertical traverses tested.

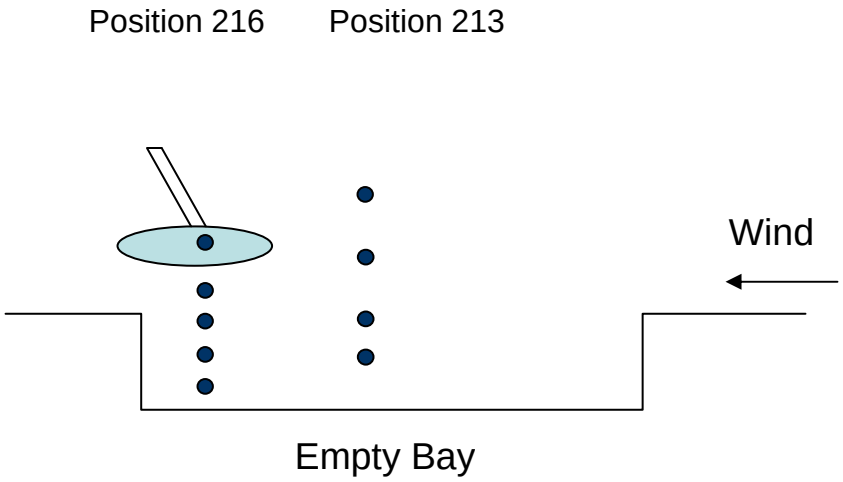


**Figure 30. Test Matrix of Vertical Traverses**

### *Mid-Cavity Traverse*

The store was placed at position 213, at the middle of the cavity. 4 different positions based upon the wind tunnel vertical traverse were tested. The positions were located at 2.1, 3.0, 3.5, and 4.5 ft from the floor of the cavity. As Figure 31 shows, the values for the pitching moment were quite different from that of the CFD. The error bars displayed signify one standard deviation above and below the averaged value. The general trends were correct, although the actual values predicted were far below the wind tunnel; under predicting the effect of the flow as compared to the wind tunnel. This poses an interesting question regarding the comparative values of the CFD as to wind tunnel studies as a function of the store's position within the cavity. Will CFD still under predict the moments when evaluating the store at the front or back of the cavity?

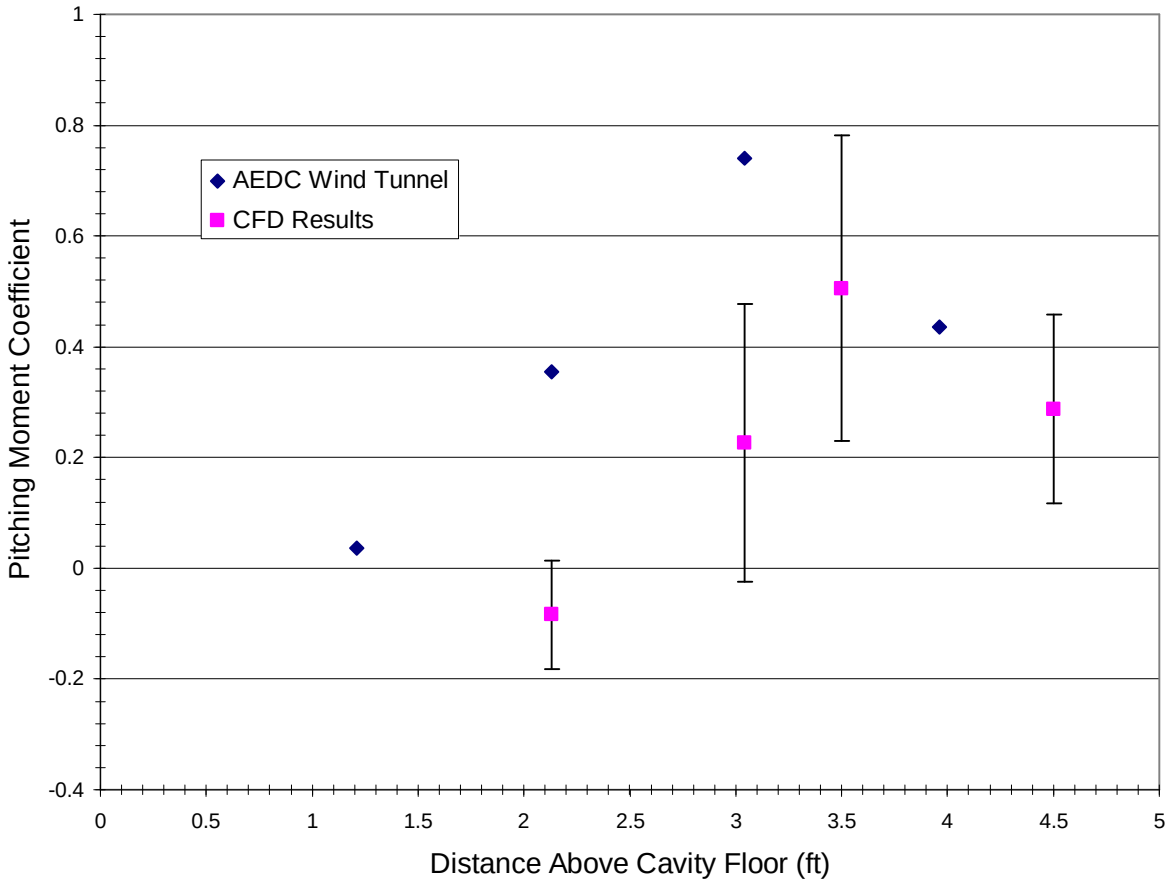


**Figure 31. Mid-Cavity Vertical Traverse Pitching Moment Comparison**

Beginning at the first position of 2.12 ft, the pitching moment coefficient is far below the wind tunnel data, to the point of being the opposite direction of that calculated by the wind tunnel. The standard deviation barely passes vertical. However, at this point in the cavity, the aerodynamics are complex and highly unsteady. Another aspect to keep in mind is that these coefficients are dependent upon the dynamic pressure, *q*, which is dependent upon the velocity of the flow. Deep within the cavity, there are issues of highly separated flow as well as very different velocities from the speed of Mach 0.85 in the freestream. The wind tunnel gives a rather large value for the pitching moment at this position, with the store completely in the cavity. This serves to show that the S-A turbulence model, as well as the semi-steady approximation of this unsteady flow do not model the interior flow in the cavity well. Also important to note is the shift in the trend, that the CFD results seem to be smaller, and if shifted to the left, would match

up much better with the wind tunnel moment. The general trend is modeled in CFD with the flow exhibiting less flow angularity, an angularity which is delayed until a point further aft of the leading edge. The standard deviation at the higher positions is quite large, on the order of ±0.2, or almost 50% of the value at that point. This suggests that the flow at this location is highly unsteady, and the 12000 iterations that resulted in fair convergence for the longitudinal traverse might not be sufficient in this case. Further study of this area of the shear layer would yield important information which could lead to a more accurate characterization of the nature of the shear layer. At the highest position, shown visually in Figure 32, the shear layer can be seen dipping into the cavity and twisting towards the store. Even at more than a diameter away from the opening, the store is influenced by and influences the shear layer.

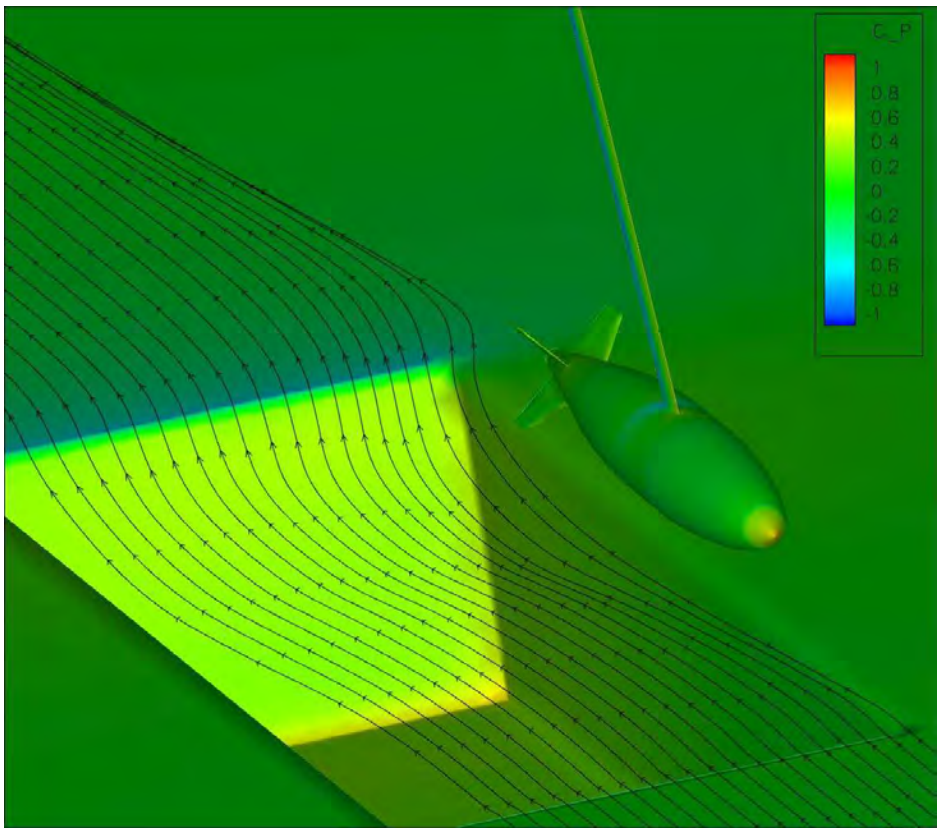


**Figure 32. Visualization of Mid-cavity Vertical Traverse**

### *Aft-most Vertical Traverse*

At this position, a total of five positions were tested, from 1.2 feet off of the cavity floor to 2.5, 3.0, 3.5 and finally 4.0 feet from the bottom, 1 foot away from the plane of the cavity opening. The traverse, as with the others, was done at 0 angle of attack and 0 sideslip. The lack of alternate angles for these positions inhibits slightly the trajectory simulation, however the challenges involved with the NAVSEP program will be evaluated later in this discussion. The progression for the pitching moments can be seen in Figure 33. When compared to the longitudinal progression of the pitching moment in Figure 28, the pitching moments vary much more, and reach the 'ripple' when coming to convergence much later. Even when they do reach that wave-like motion, the group as a whole does not parallel each other as close. This can be attributed to the extreme change in the flow when progressing from deep within the cavity to a position above the shear layer. At the position in the middle of the shear layer, along the opening at 3.04 ft, the solution does not follow a smooth curve, rather it is jagged and not coordinated with either the 2 positions below or the 2 positions above. In sum, the degree of ripple corresponds to a configuration where there is more unsteadiness in the flow. This unsteadiness is likely caused by the interaction of the store and shear layer. As seen, this interaction varies based upon the positioning of the store.

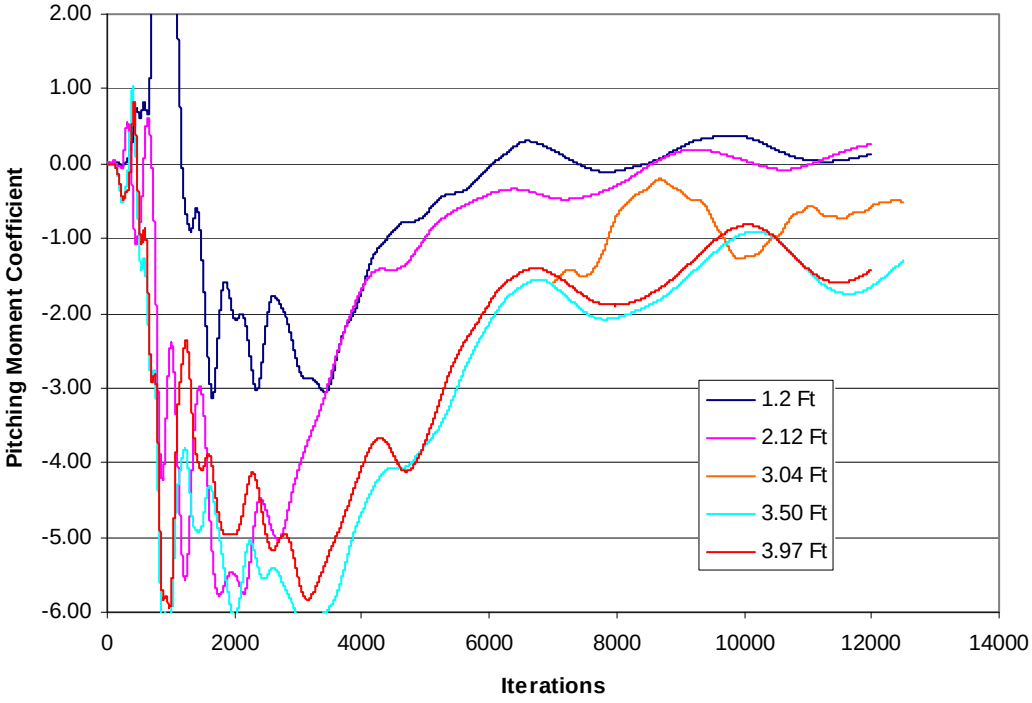


**Figure 33. Progression of Pitching Moment with Iterations**

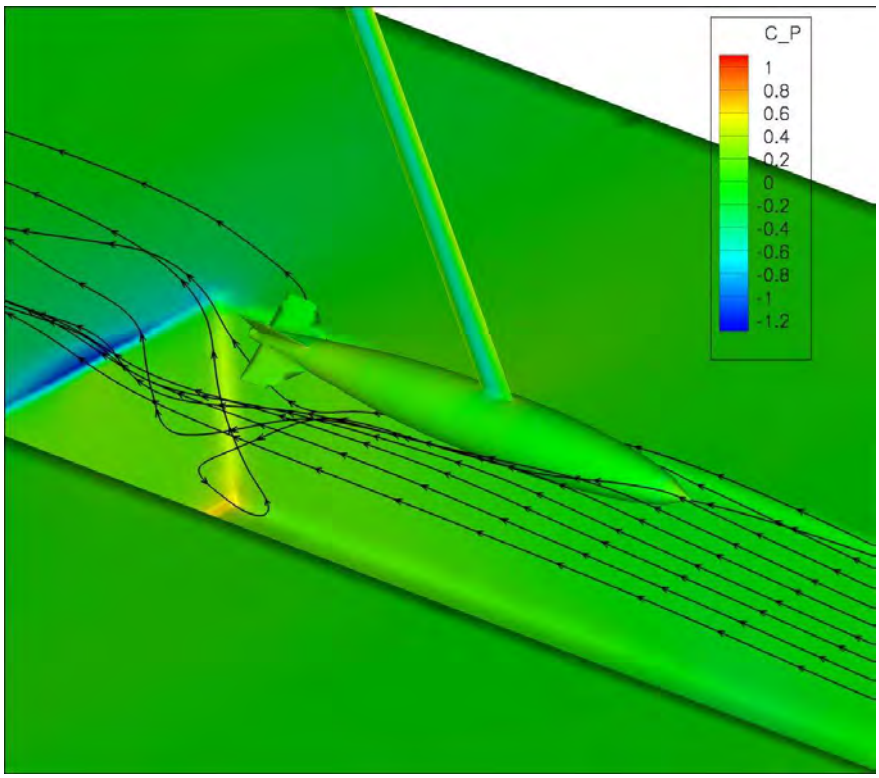


**Figure 34. Visualization of Aft-most Streamlines**

Following from the numerical data, it is not a surprise to see in Figure 34 the erratic nature of the streamlines. The few streamlines that dip deep into the cavity then shoot out at an almost vertical manner, right past the fins at the end of the store. Extrapolating from these few streamlines, it is easy to see how the airflow has a significant impact upon the store and its orientation. In Figure 35 you can see the results for the pitching moment along the z axis. The general trends of the wind tunnel data are followed by these moments as are those of the vertical traverse at position 213. However, the proximity of the values for the measurements is generally closer for the 216 position than the 213 position.

An interesting result is the point at 3.5 feet, it seems that the wind tunnel data could have skipped a local maximum in the pitching moment, one that the CFD has captured. The magnitude and location of this moment could be beneficial for future analysis. The error bars demonstrate one standard deviation, which is surprisingly small at 2.12 feet. This is similar to the results obtained at position 213, indicating that the approximation reaches a more converged state, although that convergence is much farther from the wind tunnel values than those when the

store is above the shear layer. However, when the store is above the shear layer at this position, it begins to over-predict the pitching moment, even above the standard deviation.

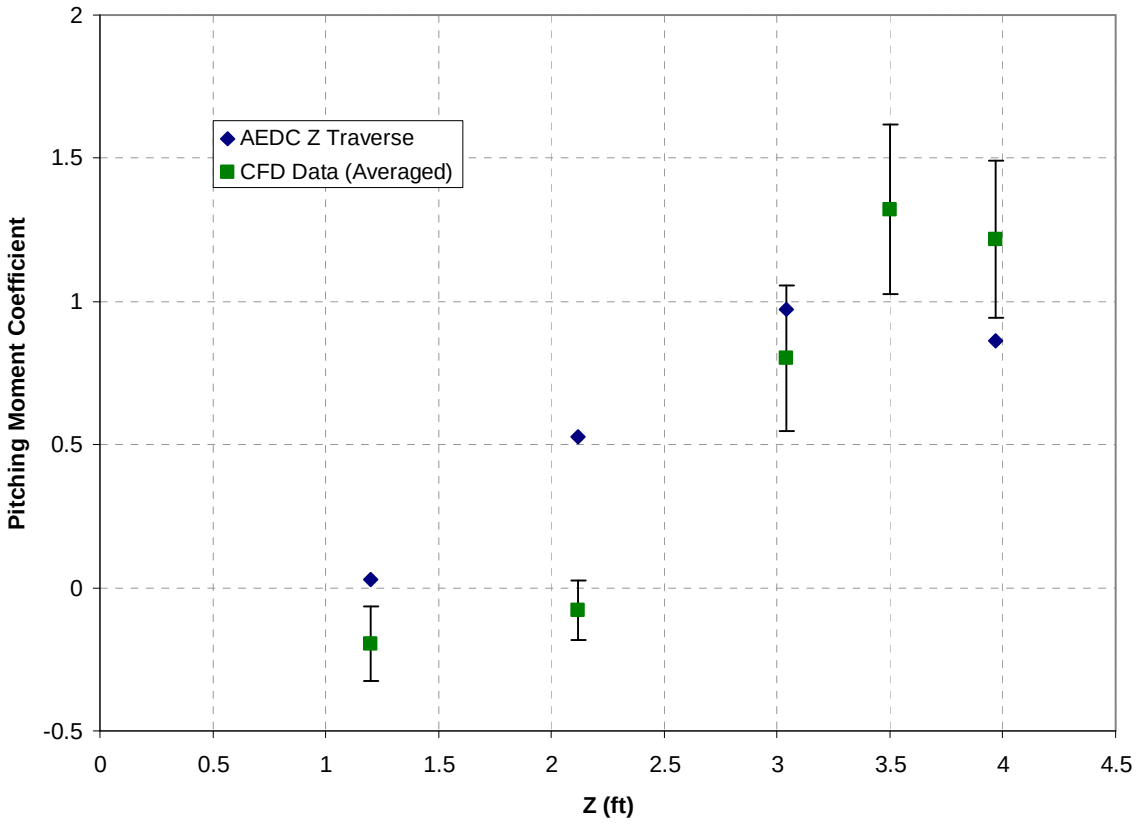


**Figure 35. Aft-most Traverse Pitching Moment Comparison**

In addition to comparing the pitching moment coefficient, it is interesting to take a look at the yawing moment coefficient as compared to wind tunnel results. As will be shown in Figure 37, the AEDC data which is compared in this graph is significantly different from other similar configurations tested in the wind tunnel.

## Discrepancies and Coefficient Analysis

The CFD calculated values for the model were compared to the wind tunnel results for that configuration, labeled as 216. As the initial results failed to match the yawing moment at all, it was clear there was an additional problem. The graphs for the yawing moment looked nothing alike when compared, and when the moments of this configuration were displayed alongside the

data calculated, the difference existed only in the yawing direction. In order to check the wind tunnel data the other 3 configurations, all of which have extra “dummy” stores in order to approximate the different loading, and effect of that loading were evaluated. These “dummy” stores are static models placed in the bay in order to simulate a full load. The configurations compared have different numbers of these static models in the cavity. This can be seen in Figure 36 and Figure 37 below.

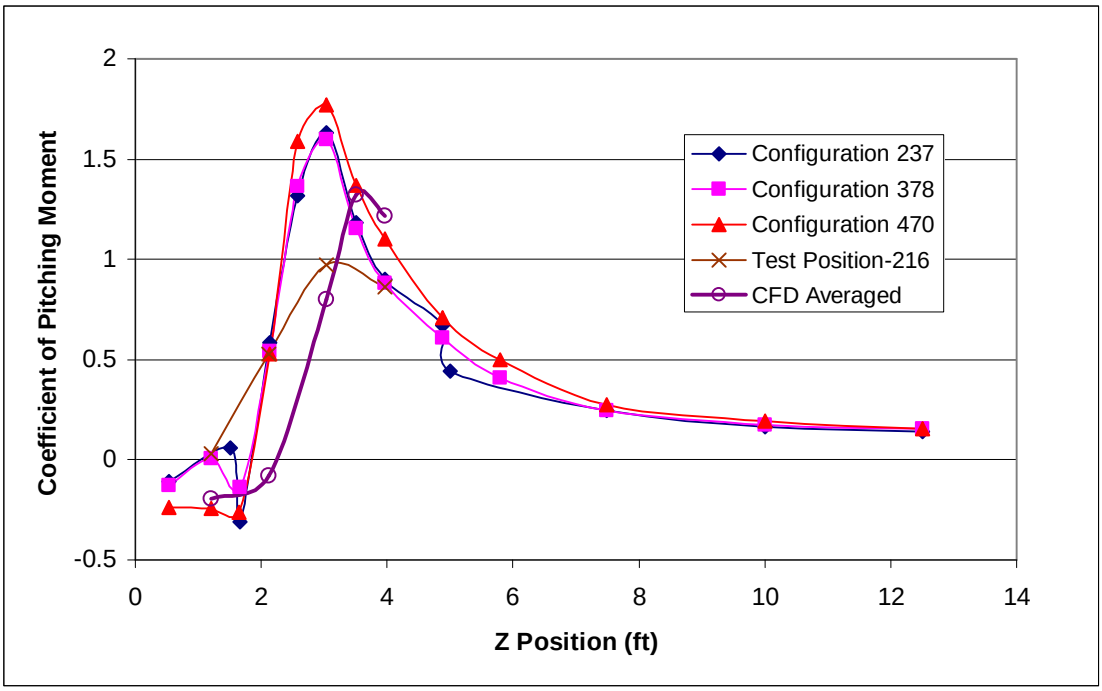


**Figure 36. Wind Tunnel Position Pitching Moment Comparison**

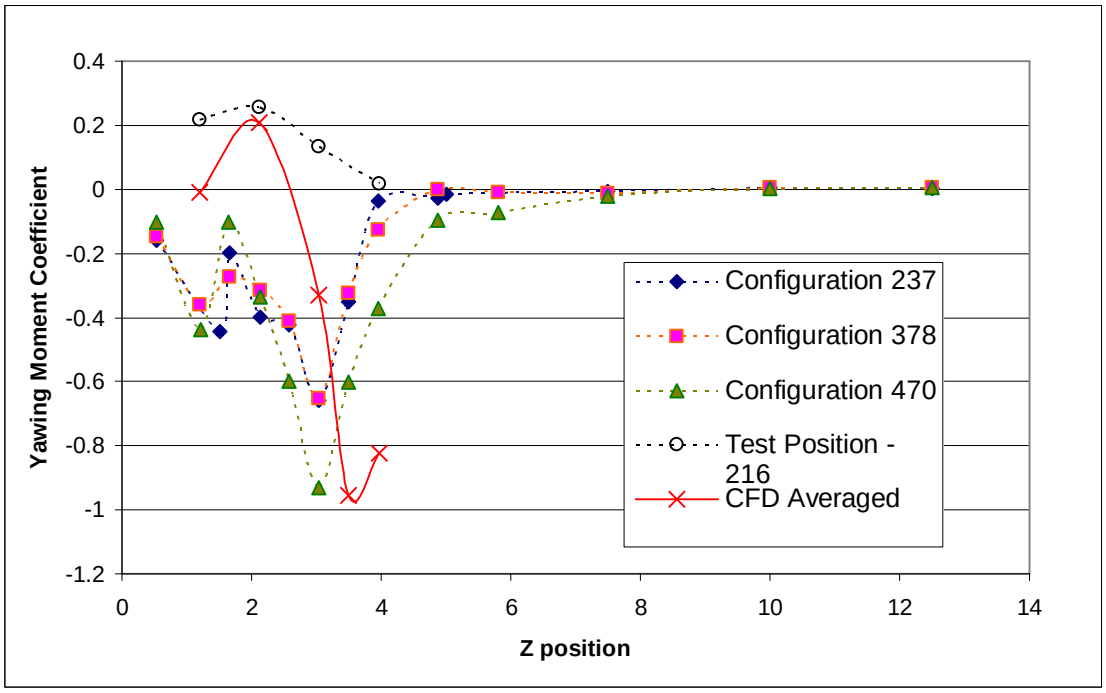


**Figure 37. Wind Tunnel Yawing Moment Comparison**

Particularly when looking at the yawing moment coefficient, the test configuration is very different from the other three configurations. In order to compare the CFD values to accurate wind tunnel forces and moments, the CFD was evaluated in comparison to configuration 237. This configuration was chosen because it only contained one dummy store as compared to two or three for 378 or 470, respectively. In all of these positions, the position of the test store with the balance apparatus was the same. This configuration is very similar to the 216 position, having the store in the same position, traversing the z axis, except for the fact that the 237 had more test points-extending past 12 feet. This both extended the range of data and allowed the store to almost reach a free-stream condition, aiding in the trajectory accuracy. With this new set of data, the coefficients were compared as shown in the three figures below. The pitching moment as well as the rolling moment compare favorably, showing the right-ward shift in the CFD pitching and rolling moment coefficients.

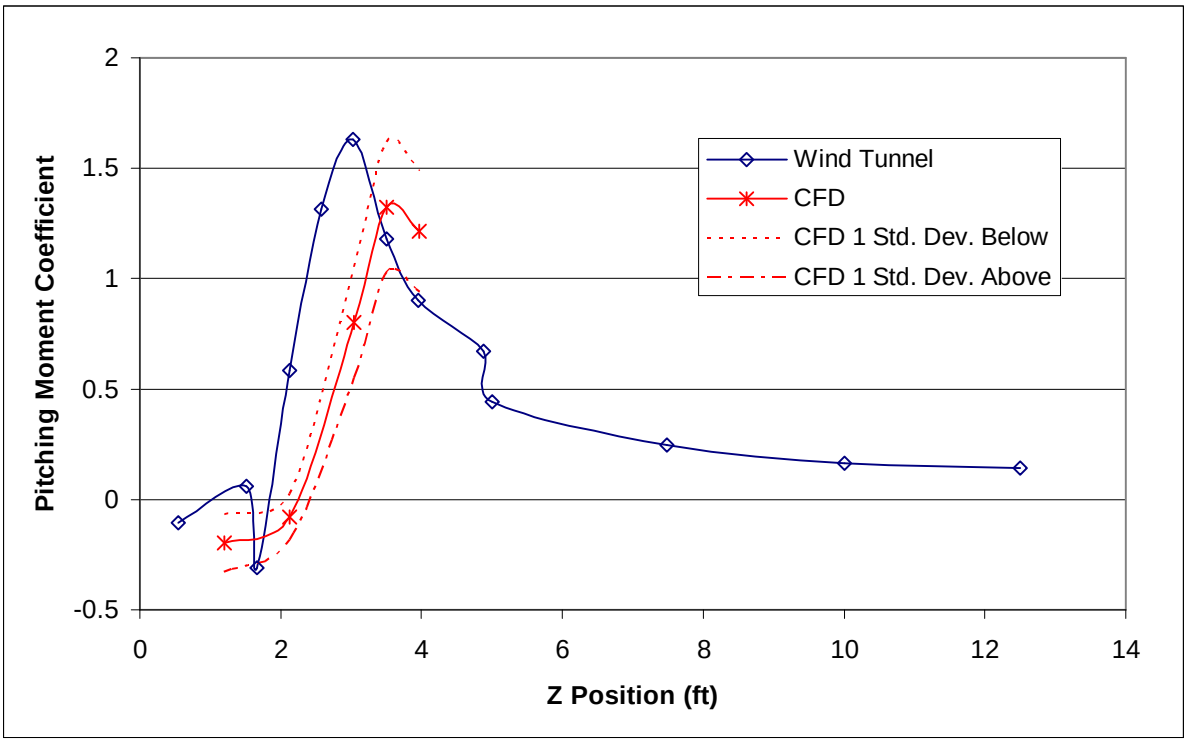


**Figure 38. Pitching Moment Comparison with Configuration 237**

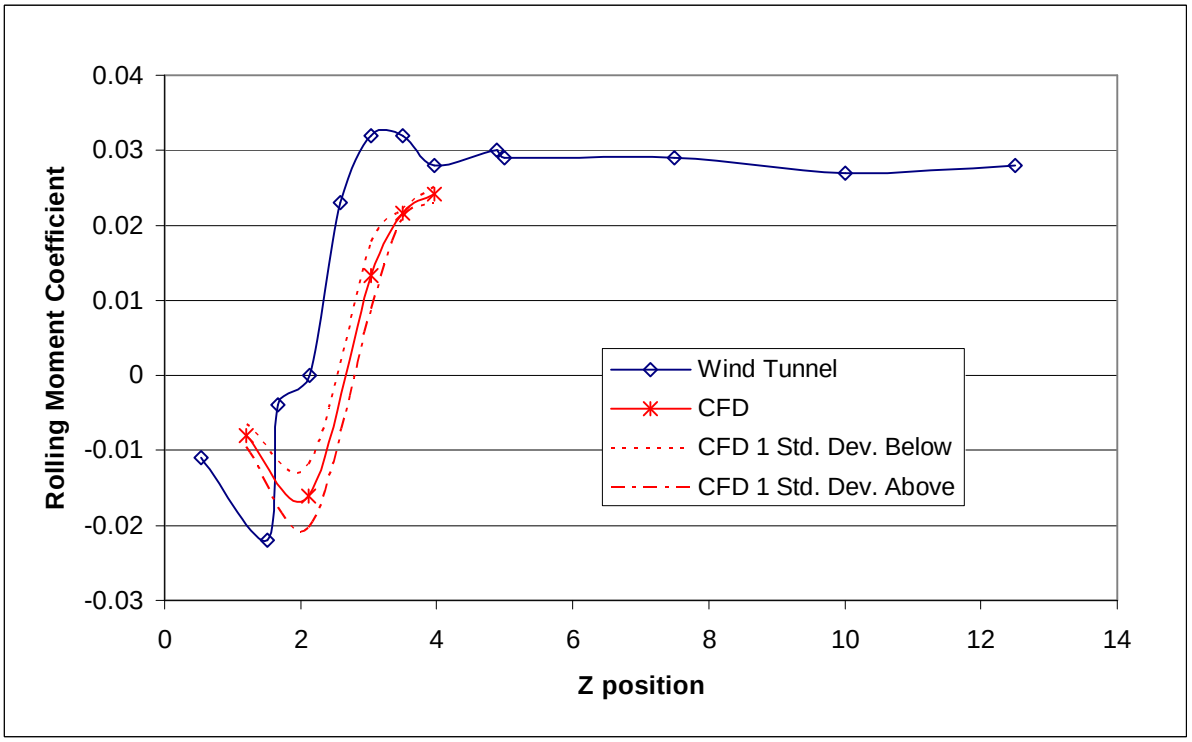


**Figure 39. Rolling Moment Comparison with Configuration 237**

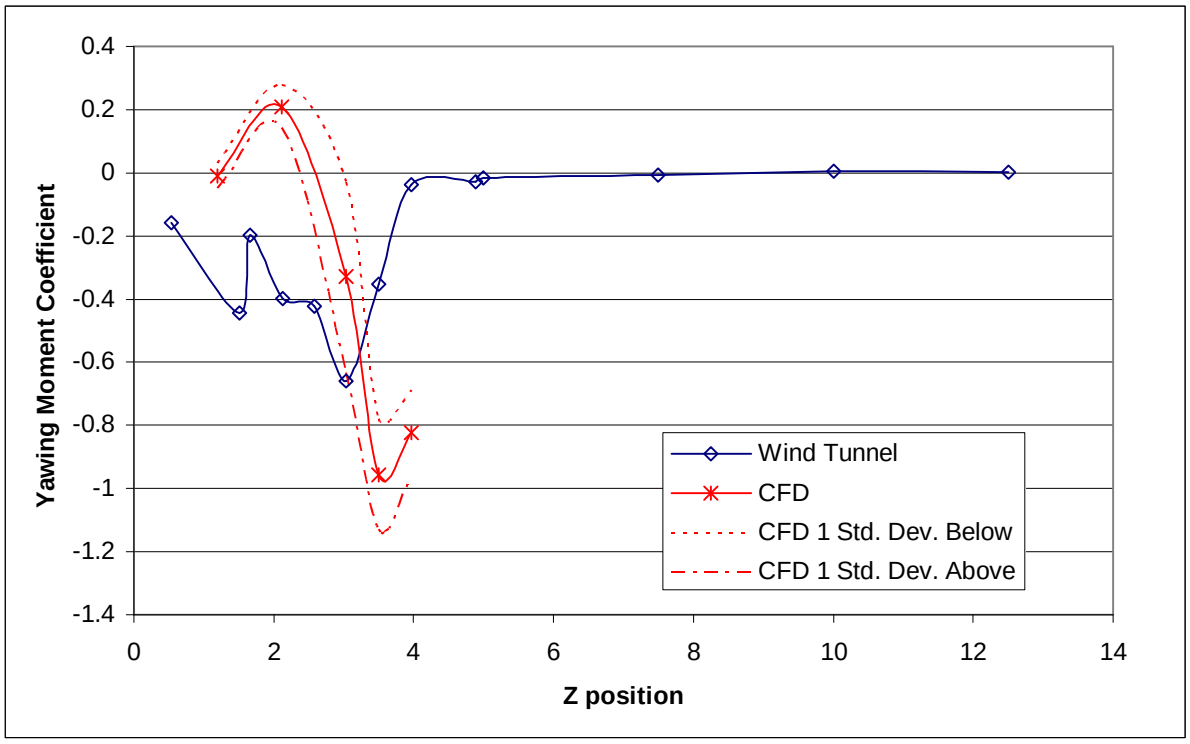


**Figure 40. Yawing Moment Comparison with Configuration 237**

The yawing moment comparison as shown in Figure 40 is the most different of the comparisons. It is clear that deep within the cavity, the approximation does not hold true for calculating the yawing moment particularly. Once outside the cavity, above 3.04, the yawing moment is over-predicted.

## NAVSEP Trajectories

Calculating the trajectories of the store based upon the different data sets helped to understand the consequences of these differences in forces and moments. This analysis revealed the suitability of CFD in predicting the trajectories. The trajectory found using the CFD values averaged over the last 3000 iterations was bounded by two other trajectories. These two were the calculated trajectories based off of the forces and moments that were at one standard deviation above and below the averaged values.

### *Angular Analysis*

The angular orientation of the store is a critical evaluation point, and one that is much easier to evaluate when the analysis is done through CFD. The orientation greatly affects the physical displacement of the store, and can be evaluated to determine causes of deviation from the translational path of the store through the air.

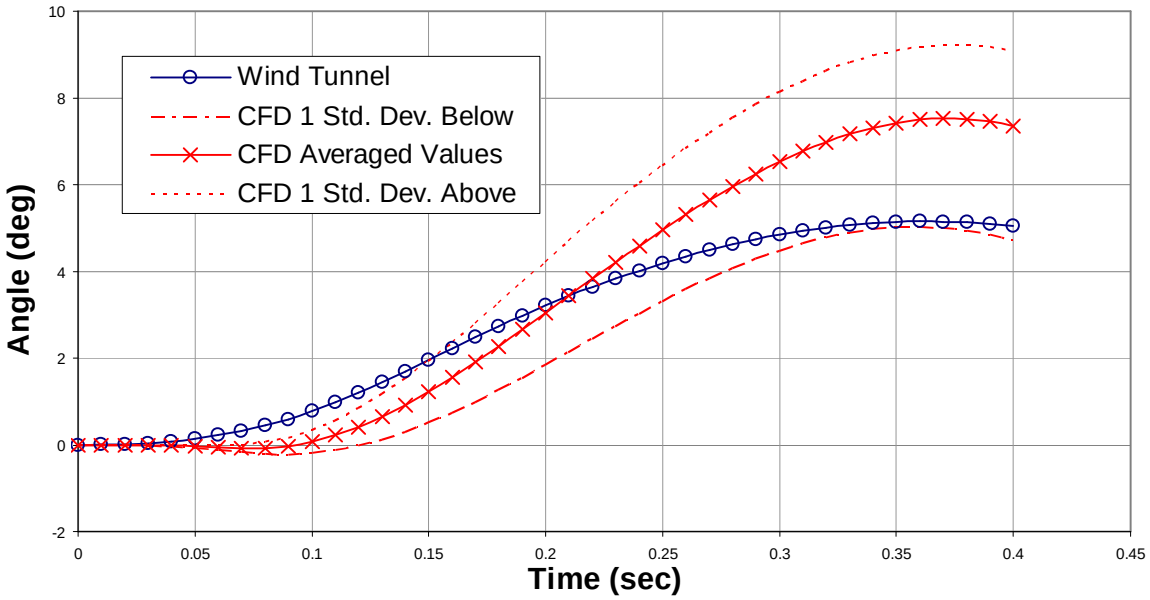


**Figure 41. Psi Analysis**

The CFD trajectory for the yawing angle, psi, matches that of the wind tunnel after some time - it doesn't have the same curvature but the wind tunnel trajectory generally stays within the bounds of the standard deviation from the CFD analysis. This is to be expected, as the initial yawing moment calculated by CFD was the opposite sign of the wind tunnel moment, evidenced by the slight dip after the 0.05 second mark. The CFD coefficient over-predicted the moment the further away from the cavity the store moved. This would stand to reason that the CFD-based trajectory would reach a larger angle. The important aspect is to note that at the 0.4 second mark, both look as if they are headed on a gradual slope downwards. This tendency to return to equilibrium indicates that the model is behaving according to basic rules of aerodynamic flow. The yawing moment is significant in the store separation clearances, and it is important that the CFD moments match with those of the wind tunnels.

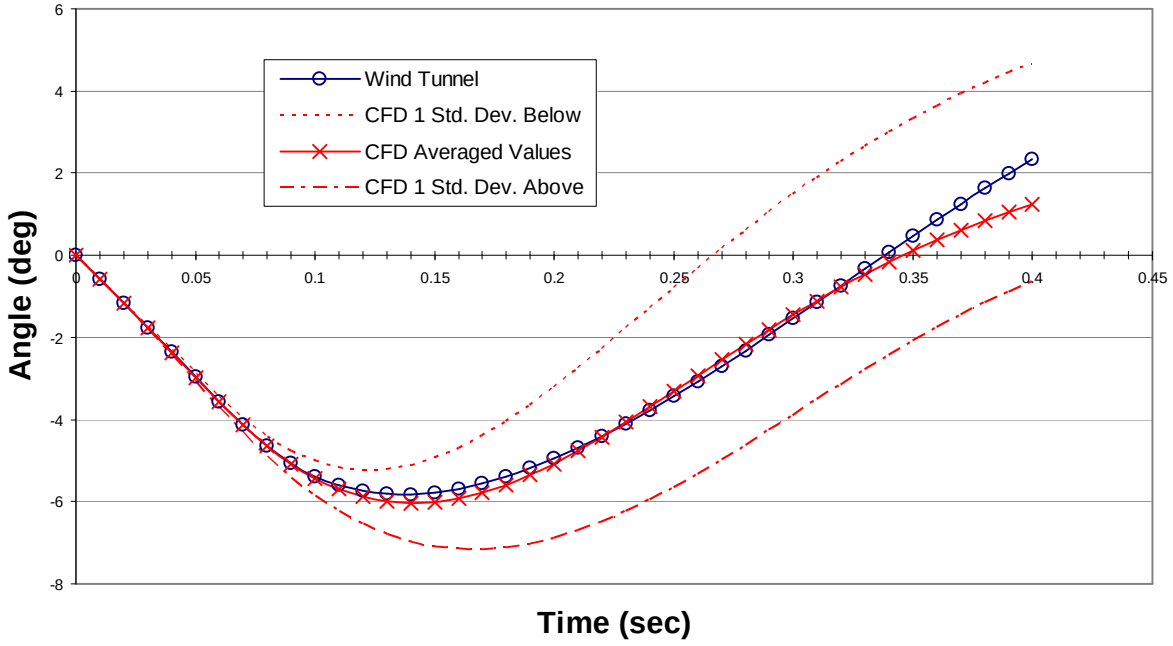


**Figure 42. Theta Analysis**

Theta, the pitch angle, is close to a perfect match, showing that despite the differences in absolute values, the trajectories are significantly similar. The trajectory follows the negative pitch down then the nose up moment, pitching it up to equilibrium. At the end of the trajectory, the CFD trajectory begins to level out to return to the equilibrium, steady state position of 0 degrees of pitch. The wind tunnel does not show the tendency to nose down, however, the dummy data point that was addressed earlier could be responsible for the early tendency to return to 0 degrees.

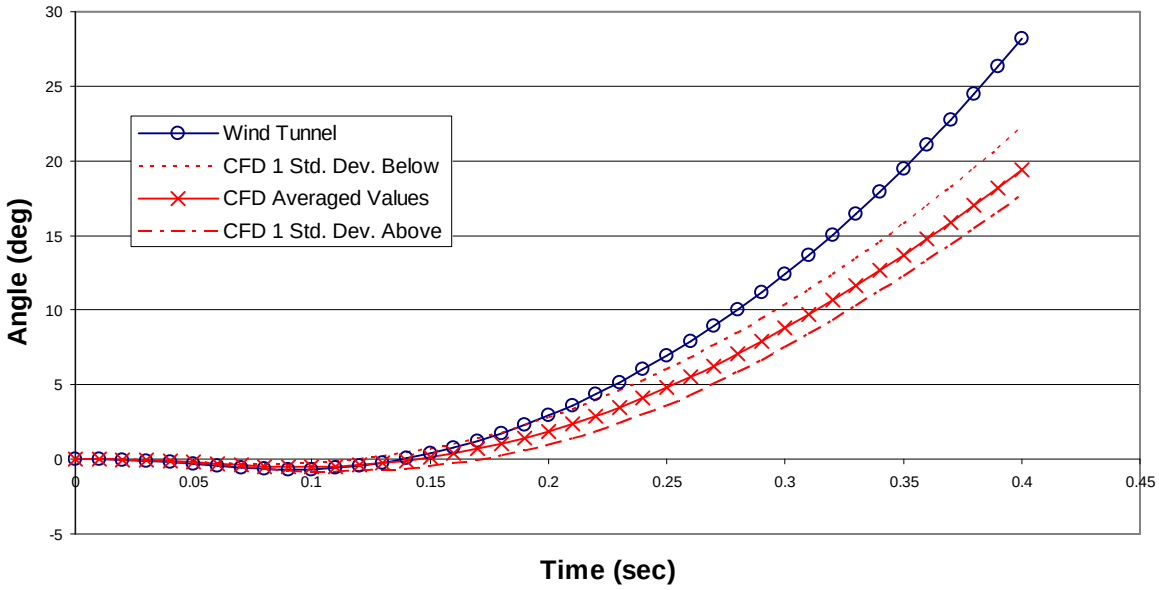


**Figure 43. Phi Analysis**

Roll angle, phi, is much higher and increasingly so; while it's the same trend, the wind tunnel is on an exponential path to increasing the roll angle. The difference in roll angles and rates is notoriously difficult to capture with CFD, and can have a large effect as will be seen in the displacement analysis. Considering Figure 39, the wind tunnel has a much higher rolling moment coefficient that is sustained throughout the traverse. It is interesting that the value doesn't return to an equilibrium position, but continues at the same value out to 6 or 8 feet beyond the cavity. The change in the fin orientation can produce some interesting 2$^{nd}$ order effects especially when the airflow around the store is turbulent and complex, as in this situation. This difference could be the cause of the discrepancy in the Y displacement prediction.

### *Displacement Analysis*

The Y displacement graph, Figure 44 shows the path of the trajectories. Not only do the paths not match up, or parallel each other, they are completely opposite. There is little displacement until the 0.2 time, and both the wind tunnel and the CFD data show the store

moving towards the center of the cavity. The CFD trajectory levels out and begins to move towards the side of the cavity while the wind tunnel moments resulted in an increased rate of movement towards the center of the cavity. The possible reason for this discrepancy can be seen in Figure 45. The normal force coefficients as predicted by the NAVSEP program are diametrically opposed. A further look into the calculated CFD coefficients can be seen in Figure 46. The CFD data is compared with two configurations besides 237 to gain perspective on this particular measurement. The CFD data is far from close to any of the configurations, at its max reaching three times the magnitude of the highest value obtained by the wind tunnel configurations. Clearly the problem seen in Figure 44 as the trajectory difference can be traced back to the side force calculations seen in Figure 45 and finally back to the beginning with the flow solution in Figure 46. Evidently the approximation made with the S-A turbulence model had difficulties resolving the side force coefficients.

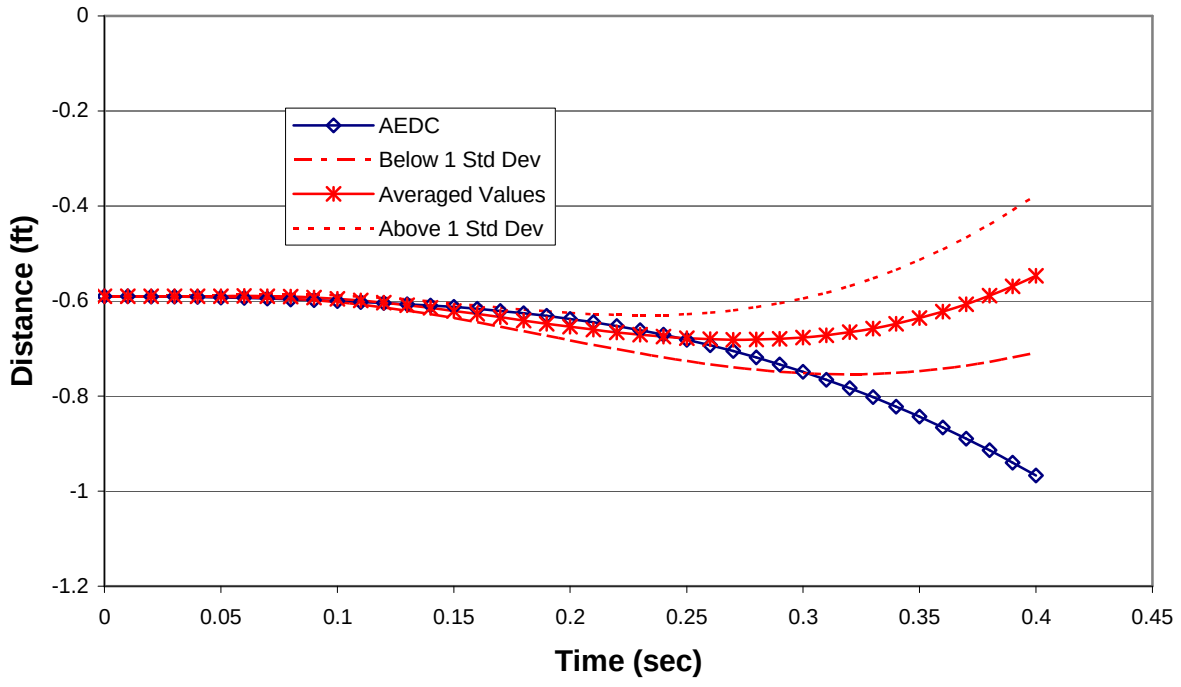


**Figure 44. Y-axis analysis**

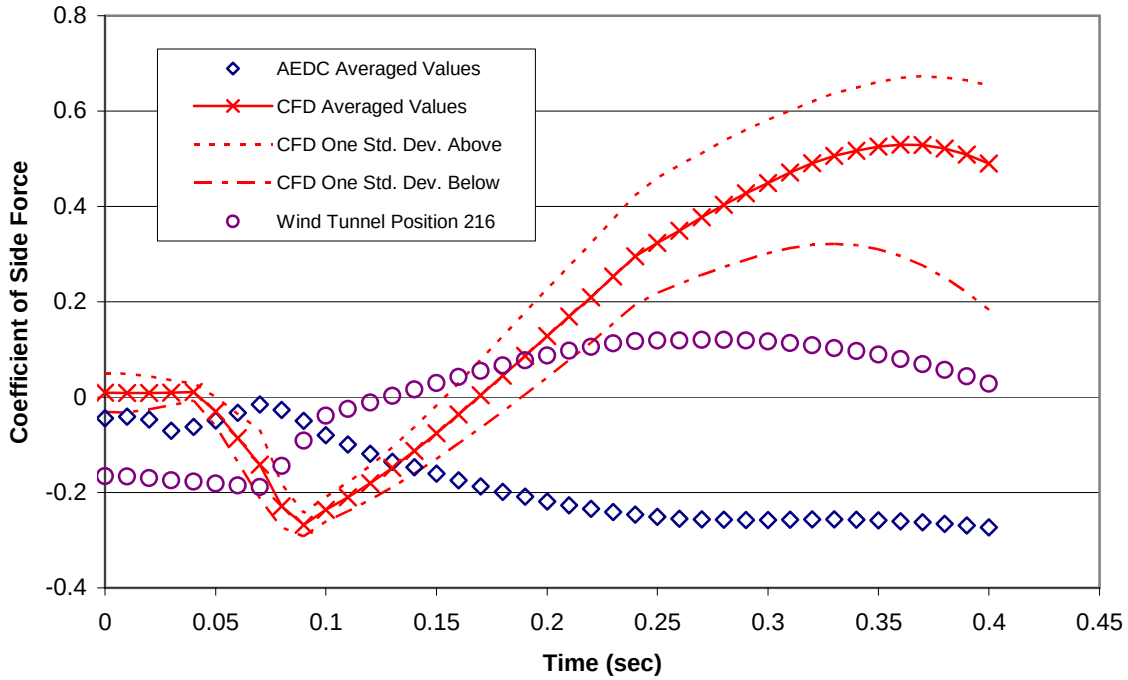


**Figure 45. Side Force Coefficient from Trajectory Calculation**

As seen in the analysis, the angles describing the orientation of the store, or Euler angles, are in good agreement from CFD to wind tunnel. However, the side force coefficient difference indicates that the simulated side slip angle is much higher in CFD than in the wind tunnel. Based upon these two observations, the increased flow angularity can not be over the tail, as this would result in a large yawing moment and in significant differences in the yaw angle. This was not the case therefore the increased flow must be on the forward section of the store.

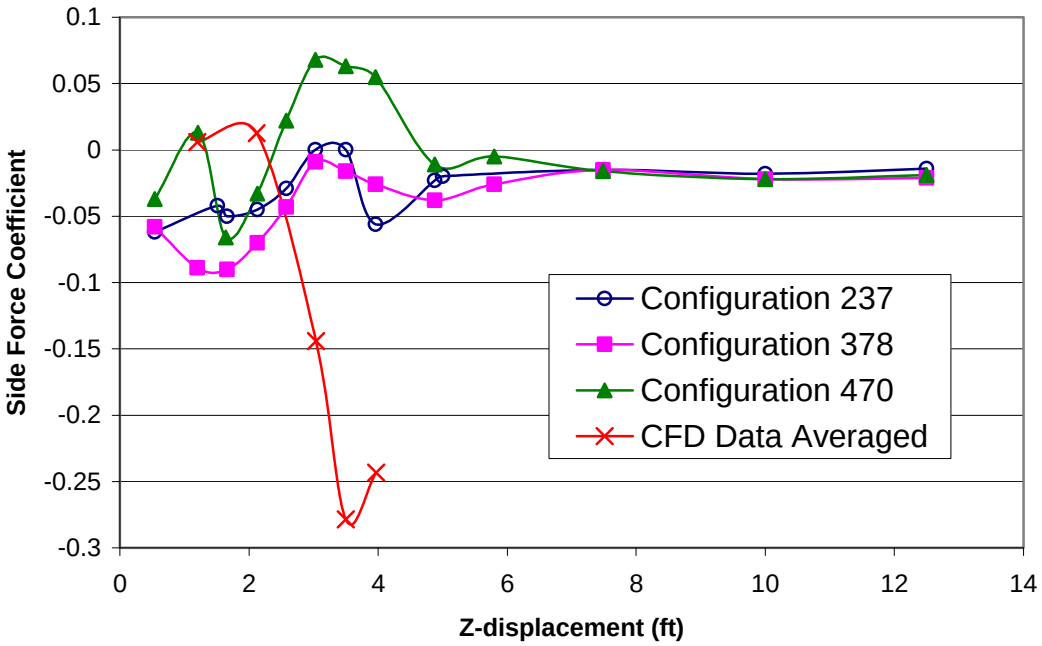


**Figure 46. Side Force Coefficients from Wind Tunnel and CFD**

From analysis of the X and Z displacements in Figure 47 and Figure 48, the path of the store based upon wind tunnel data and CFD data are almost the same. This shouldn't be much different for the Z displacement, as the stores are ejected out at the same high velocity. The comparison of the X displacement is much the same, as it is difficult to accurately solve for the drag in CFD. As a result, the inputs to the NAVSEP program deliberately decrease the influence of the drag coefficients from the CFD test.

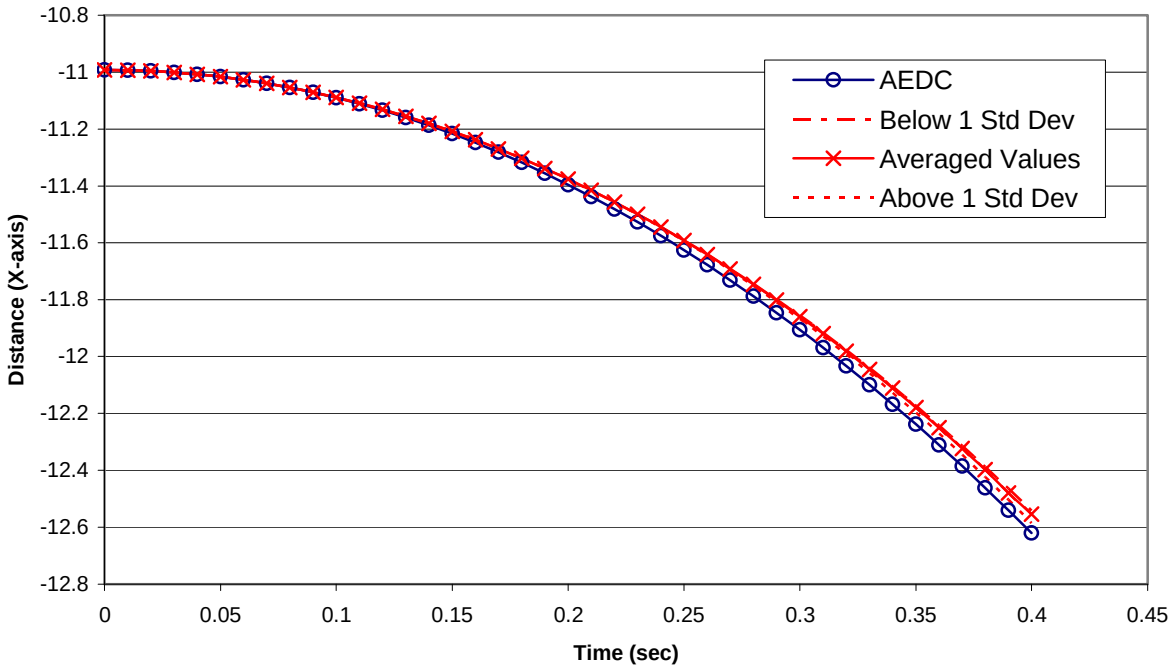


**Figure 47. X-axis analysis**

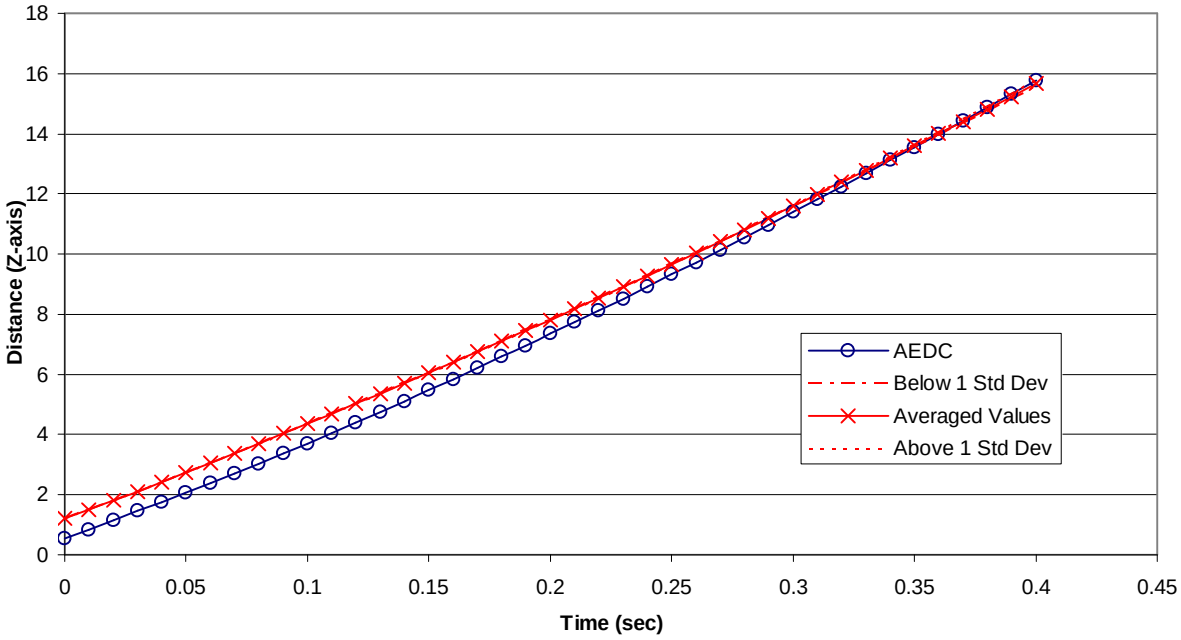


**Figure 48. Z-axis analysis**

Raw data from the trajectory solutions can be found in Appendix A.

## Evaluation of Future Analysis

It is also possible to use the USM3D flow solver to compute the time-accurate flow over a geometry. When the flow is steady, this method should converge to the solution previously addressed. In the case of large areas of flow separation, the flow may not be steady. In that case, the force on the store in the unsteady flow will fluctuate. It is hypothesized that the mean value of this fluctuation should match measured wind tunnel data since the wind tunnel returns time averaged load data. Furthermore, it is thought that an analysis of the fluctuations can be used to bracket the 'unsteadiness' in the flow, at least in terms of its effect on the store. This bracketing will have a role to play in the parametric analysis of the stores trajectory. Additionally, it would be interesting to test additional flow solving methods and approximations on this same problem in order to determine the method that would result in the values closest to the wind tunnel data.

Once a method is found that will approximate the wind tunnel data more closely, the CFD calculations could be used with the NAVSEP program to determine the minimum ejector force needed to eject the stores safely. As electronics get more and more sophisticated, the high forces that accompany the ejection could damage them. By calculating this minimum force needed, more sophisticated electronics can safely be used in the guidance systems for stores dropped out of internal bays. However, this is something that is difficult to model in a wind tunnel and would be beneficial information for future development. As provided by experts at the ITEA conference, the Spalart Allmaras turbulence model now has been combined with the detached eddy simulation (DES) to account for the irregularity of the flow swirling in the cavity. This is just one example of the numerous other turbulence models that are available to test in this configuration. As this, one of the simpler models, could not approximate the trajectory with a high enough accuracy, the other models should be attempted in order of increasing complexity in order to ensure that the most practical and time efficient process is found. At the far end of the spectrum is the time accurate solutions, which would be useful in characterizing the forces and evaluating whether the very time-intensive solutions yield an accurate estimation as compared to the wind tunnel testing. However, this would be the least practical method tested, and would serve only to validate the possibility of CFD matching correctly the wind tunnel data.

## Computational Hours

Due to the parallel processing, solving each configuration was reasonable, with an 8000 iteration run taking approximately 13 hours. To date, 15 different configurations of cavity and Mk-82 were run. In addition, there were 32 different configurations for the model validation run on the JAWS supercomputer at the Maui High Performance Computing Center. A rough estimate of the total computer time is approximately 8000 processor-hours used, with 3450 processor-hours from the work at the Naval Academy and 4550 from the summer internship.

# CONCLUSIONS

The NICS wind tunnel tests represent a unique cavity store test where the forces and moments on the store were measured along a longitudinal traverse at the opening of the bay. An unstructured CFD study was conducted modeling the aerodynamics of flow in the vicinity of the store along the traverse using a steady-state approach. Preliminary CFD results indicated that the faired strut used to position the store inside the bay did not have a large influence on the force measurements on the store but that an un-modeled part of the apparatus did as indicated by the wind tunnel data, at least at store angles of attack above approximately 10 degrees. Force measurements on the store using CFD were in qualitative agreement with the wind tunnel tests, both showing increasing pitching moments away from the opening of the bay as the store is positioned aft in the opening. CFD measurements under predicted the magnitude of the pitching moment by approximately 50% at each station. These differences were not as significant in the trajectory simulation however. The trajectory predicted from the wind tunnel data fell within the standard deviation bounds for the CFD data in every parameter except for the y-axis displacement. CFD can be used as a rough estimate of the trajectory but is not accurate enough to be used to certify store releases or establish test sequences. The shear layer has been characterized both horizontally and vertically, at the middle and the rear.

## Future Work

The piece of this analysis missing the most is the evaluation through other approximations. If possible to use this same set of data and calculate the solution based upon some other method, the comparisons could begin for which program is the most accurate with this sort of problem. The time-averaged solution would also be a great data point through which the semi-steady solutions could be evaluated.

## Recommendations

By modeling the strut on the store, it was possible to determine things that the wind tunnel would not show. Small details such as the measuring apparatus build the case for

conducting parallel CFD-wind tunnel tests for initial checking against the different apparatus' used in the wind tunnel. In order to learn more about the models and the flow being tested in high-caliber wind tunnels, CFD should be used more extensively as a tool to double-check the legitimacy of some statements. In addition, the mid-section of the cavity seems to be the source or beginning of most of the problems. If a more detailed study was done on that physical area details describing the shear layer flow and other pertinent information could be determined.

# BIBLIOGRAPHY

Anderson, John D., Computational Fluid Dynamics: The Basics with Applications. New York: McGraw-Hill, Inc., 1995.

Cenko, A., "Experience in the Use of Computational Aerodynamics to Predict Store Release Characteristics," *Progress in Aerospace Sciences*, Vol. 37, 2001, pp. 477-495.

Cenko, A., "F-18/JDAM CFD Challenge Wind Tunnel Flight Test Results," AIAA Paper 99-0120, Jan. 1999.

Frink, Neal, et. al., "TetrUSS," http://aaac.larc.nasa.gov/tsab/tetruss/mac/TetrUSS-2005-0812.pdf. October 2006, (October 2007).

Lee, Youngki, Kang, Minsung, Kim, Heuydong, and Setoguchi, Toshiaki., "Passive Control Techniques to Alleviate Supersonic Cavity Flow Oscillation," *Journal of Propulsion and Power,* Vol. 24, No. 4, July-August 2008 pp. 697-703.

MacManus, David G., and Doran, Diane S. "Passive Control of Transonic Cavity Flow," *Journal of Fluids Engineering*, Vol. 130, June 2008, 064501.

Mani, M., Cary, A., and Ramakrishnan, S.V., "A General Purpose Euler and Navier-Stokes Solver for Structured and Unstructured Grids," *Journal of Aircraft*, Vol. 42, No. 4, 2005, pp. 991-997.

Murman, S.M., Aftosmis, M.J., and Berger, M.J., "Simulations of Store Separation from an F/A-18 with a Cartesian Method," *Journal of Aircraft*, Vol. 41, No. 4, 2004, pp. 870-878.

Niewoehner, R.J., and Filbey, J., "Computational Study of F/A-18 E/F Abrupt Wing Stall in the Approach Configuration," *Journal of Aircraft*, Vol. 42, No. 6, 2005, pp. 1516-1522.

Parikh, P., and Chung, J., "Computational Study of the Abrupt-Wing- Stall Characteristics of F/A-18E and F-16C," *Journal of Aircraft*, Vol. 42, No. 3, 2005, pp. 600–605.

Pirzadeh, S., "Unstructured Viscous Grid Generation by Advancing-Front Method," NASA Contractor Report 191449, 1993.

Rothback, N., and Cenko, A., "Dangers of Aircraft Modifications Without Conducting an Investigation into the Effects on the Aircraft Flowfield and Flying Qualities," 2001, pp. 1-14.

Sadeh, Y., and Gaton, V.A., "F-16/SPICE Separation Analysis-Summary of the Risk-Reduction Phase Program," *Journal of Aircraft*, Vol. 40, No. 1, 2003, pp. 70-76.

Sinha, N., Arunajatesan, S., and Ukeiley, L.S., “High Fidelity Simulation of Weapons Bay Aeroacoustics and Active Flow Control,” AIAA Paper 2000-1968

# APPENDIX A:

CFD Solution (average of last 3000 runs)

30 LB Ejector Force

| FLIGHT TIME (sec) | AXIS XF (ft) | POSITIONS YF (ft) | AND ZF (ft) | ORIENTATIONS PSIF (deg) | THAF (deg) | PHIF (deg) |
|---|---|---|---|---|---|---|
| 0 | -10.992 | -0.59 | 1.2 | 0 | 0 | 0 |
| 0.01 | -10.993 | -0.59 | 1.5016 | 0 | -0.5793 | -0.0066 |
| 0.02 | -10.9959 | -0.5899 | 1.8064 | -0.0001 | -1.1705 | -0.0269 |
| 0.03 | -11.0007 | -0.5898 | 2.1146 | -0.003 | -1.7709 | -0.0645 |
| 0.04 | -11.0075 | -0.5897 | 2.4262 | -0.0128 | -2.3768 | -0.1244 |
| 0.05 | -11.0162 | -0.5896 | 2.7412 | -0.0327 | -2.9837 | -0.2093 |
| 0.06 | -11.0269 | -0.5895 | 3.0595 | -0.0565 | -3.577 | -0.308 |
| 0.07 | -11.0395 | -0.5898 | 3.381 | -0.0729 | -4.1376 | -0.4024 |
| 0.08 | -11.054 | -0.5907 | 3.7054 | -0.0691 | -4.6455 | -0.4756 |
| 0.09 | -11.0704 | -0.5924 | 4.0324 | -0.0232 | -5.0791 | -0.5163 |
| 0.1 | -11.0887 | -0.5952 | 4.3618 | 0.0765 | -5.4273 | -0.5184 |
| 0.11 | -11.1088 | -0.5988 | 4.6936 | 0.2253 | -5.693 | -0.4784 |
| 0.12 | -11.1308 | -0.6033 | 5.0281 | 0.4188 | -5.88 | -0.3953 |
| 0.13 | -11.1547 | -0.6085 | 5.3653 | 0.6529 | -5.9924 | -0.2685 |
| 0.14 | -11.1805 | -0.6143 | 5.7055 | 0.9231 | -6.0344 | -0.0974 |
| 0.15 | -11.2082 | -0.6206 | 6.0486 | 1.2248 | -6.0105 | 0.1188 |
| 0.16 | -11.2378 | -0.6272 | 6.3947 | 1.5533 | -5.9251 | 0.3804 |
| 0.17 | -11.2694 | -0.634 | 6.7441 | 1.9039 | -5.7833 | 0.6881 |
| 0.18 | -11.3028 | -0.6408 | 7.0967 | 2.2717 | -5.59 | 1.0421 |
| 0.19 | -11.3383 | -0.6476 | 7.4526 | 2.6522 | -5.3509 | 1.4425 |
| 0.2 | -11.3756 | -0.6541 | 7.8119 | 3.0408 | -5.0718 | 1.889 |
| 0.21 | -11.415 | -0.6602 | 8.1745 | 3.4333 | -4.7588 | 2.3813 |
| 0.22 | -11.4563 | -0.6659 | 8.5406 | 3.8255 | -4.4188 | 2.9186 |
| 0.23 | -11.4996 | -0.6708 | 8.9101 | 4.2135 | -4.0586 | 3.5002 |
| 0.24 | -11.545 | -0.675 | 9.2831 | 4.5927 | -3.6855 | 4.1259 |
| 0.25 | -11.5923 | -0.6782 | 9.6595 | 4.9589 | -3.307 | 4.7956 |
| 0.26 | -11.6417 | -0.6803 | 10.0393 | 5.3097 | -2.9275 | 5.509 |
| 0.27 | -11.6931 | -0.6814 | 10.4224 | 5.6438 | -2.55 | 6.265 |
| 0.28 | -11.7466 | -0.6811 | 10.8086 | 5.9591 | -2.1767 | 7.0625 |
| 0.29 | -11.8021 | -0.6795 | 11.198 | 6.2531 | -1.8103 | 7.9002 |
| 0.3 | -11.8597 | -0.6765 | 11.5904 | 6.5234 | -1.4533 | 8.7766 |
| 0.31 | -11.9194 | -0.6718 | 11.9857 | 6.7676 | -1.1083 | 9.6901 |
| 0.32 | -11.9813 | -0.6656 | 12.3837 | 6.9828 | -0.7772 | 10.6394 |
| 0.33 | -12.0452 | -0.6576 | 12.7846 | 7.166 | -0.4618 | 11.6234 |
| 0.34 | -12.1113 | -0.6477 | 13.1881 | 7.3143 | -0.1635 | 12.6412 |
| 0.35 | -12.1796 | -0.636 | 13.5942 | 7.4253 | 0.1165 | 13.692 |
| 0.36 | -12.2501 | -0.6223 | 14.0029 | 7.4963 | 0.3776 | 14.7747 |
| 0.37 | -12.3228 | -0.6066 | 14.4141 | 7.525 | 0.6199 | 15.8885 |
| 0.38 | -12.3976 | -0.5888 | 14.8278 | 7.5095 | 0.8437 | 17.0327 |

| | | | | | | |
|---|---|---|---|---|---|---|
| 0.39 | -12.48 | -0.569 | 15.2439 | 7.4484 | 1.0496 | 18.2067 |
| 0.4 | -12.554 | -0.5471 | 15.6624 | 7.3412 | 1.2384 | 19.4103 |

AEDC Wind Tunnel Data

30 LB Ejector Force

| FLIGHT TIME (sec) | AXIS XF (ft) | POSITIONS YF (ft) | AND ZF (ft) | ORIENTATIONS PSIF (deg) | THAF (deg) | PHIF (deg) |
|---|---|---|---|---|---|---|
| 0 | -10.992 | -0.59 | 0.54 | 0 | 0 | 0 |
| 0.01 | -10.993 | -0.5901 | 0.8414 | -0.0043 | -0.5781 | -0.0114 |
| 0.02 | -10.9959 | -0.5904 | 1.1458 | -0.0174 | -1.1658 | -0.0459 |
| 0.03 | -11.0007 | -0.5909 | 1.4531 | -0.043 | -1.7605 | -0.1067 |
| 0.04 | -11.0075 | -0.5915 | 1.7636 | -0.0871 | -2.3587 | -0.1981 |
| 0.05 | -11.0162 | -0.5924 | 2.0774 | -0.1515 | -2.9595 | -0.3166 |
| 0.06 | -11.0268 | -0.5935 | 2.3946 | -0.2297 | -3.5609 | -0.4395 |
| 0.07 | -11.0395 | -0.5949 | 2.7158 | -0.325 | -4.1351 | -0.5569 |
| 0.08 | -11.0541 | -0.5964 | 3.0417 | -0.4428 | -4.6461 | -0.6492 |
| 0.09 | -11.0709 | -0.5982 | 3.3728 | -0.5898 | -5.0636 | -0.6918 |
| 0.1 | -11.0898 | -0.6 | 3.7093 | -0.774 | -5.3769 | -0.672 |
| 0.11 | -11.1109 | -0.6019 | 4.051 | -0.9869 | -5.5963 | -0.5858 |
| 0.12 | -11.1341 | -0.604 | 4.3978 | -1.2151 | -5.7365 | -0.4355 |
| 0.13 | -11.1594 | -0.6064 | 4.7498 | -1.4505 | -5.8082 | -0.2255 |
| 0.14 | -11.1868 | -0.6092 | 5.1067 | -1.6954 | -5.8184 | 0.0452 |
| 0.15 | -11.2163 | -0.6124 | 5.4684 | -1.9538 | -5.774 | 0.3784 |
| 0.16 | -11.248 | -0.6162 | 5.8349 | -2.2205 | -5.682 | 0.7734 |
| 0.17 | -11.2817 | -0.6206 | 6.2058 | -2.4831 | -5.5496 | 1.2271 |
| 0.18 | -11.3175 | -0.6255 | 6.5812 | -2.7364 | -5.3809 | 1.7383 |
| 0.19 | -11.3554 | -0.6311 | 6.961 | -2.9796 | -5.1789 | 2.307 |
| 0.2 | -11.3954 | -0.6375 | 7.345 | -3.2119 | -4.9465 | 2.9333 |
| 0.21 | -11.4374 | -0.6446 | 7.7331 | -3.4326 | -4.6869 | 3.6172 |
| 0.22 | -11.4814 | -0.6525 | 8.1253 | -3.6413 | -4.4035 | 4.3592 |
| 0.23 | -11.5275 | -0.6612 | 8.5214 | -3.8377 | -4.0988 | 5.1595 |
| 0.24 | -11.5756 | -0.6708 | 8.9213 | -4.0215 | -3.7747 | 6.0181 |
| 0.25 | -11.6258 | -0.6814 | 9.325 | -4.1924 | -3.4334 | 6.9353 |
| 0.26 | -11.678 | -0.6928 | 9.7323 | -4.3499 | -3.0768 | 7.9113 |
| 0.27 | -11.7322 | -0.7053 | 10.1432 | -4.4938 | -2.707 | 8.9463 |
| 0.28 | -11.7884 | -0.7188 | 10.5575 | -4.6238 | -2.3265 | 10.0407 |
| 0.29 | -11.8466 | -0.7333 | 10.9752 | -4.7398 | -1.9371 | 11.1952 |
| 0.3 | -11.9068 | -0.7489 | 11.3961 | -4.8418 | -1.5409 | 12.411 |
| 0.31 | -11.969 | -0.7655 | 11.8202 | -4.93 | -1.1398 | 13.6893 |
| 0.32 | -12.0333 | -0.7833 | 12.2473 | -5.004 | -0.7357 | 15.031 |
| 0.33 | -12.0996 | -0.8021 | 12.6773 | -5.0635 | -0.3308 | 16.4374 |
| 0.34 | -12.1679 | -0.8221 | 13.1102 | -5.108 | 0.0726 | 17.9099 |
| 0.35 | -12.2382 | -0.8433 | 13.5458 | -5.1372 | 0.4721 | 19.45 |
| 0.36 | -12.3105 | -0.8657 | 13.9841 | -5.1509 | 0.8657 | 21.0588 |
| 0.37 | -12.3849 | -0.8893 | 14.4249 | -5.149 | 1.2513 | 22.7379 |
| 0.38 | -12.4613 | -0.9141 | 14.8681 | -5.1316 | 1.6267 | 24.4885 |
| 0.39 | -12.5398 | -0.9401 | 15.3137 | -5.0988 | 1.9899 | 26.312 |
| 0.4 | -12.6203 | -0.9673 | 15.7616 | -5.0508 | 2.3388 | 28.2098 |